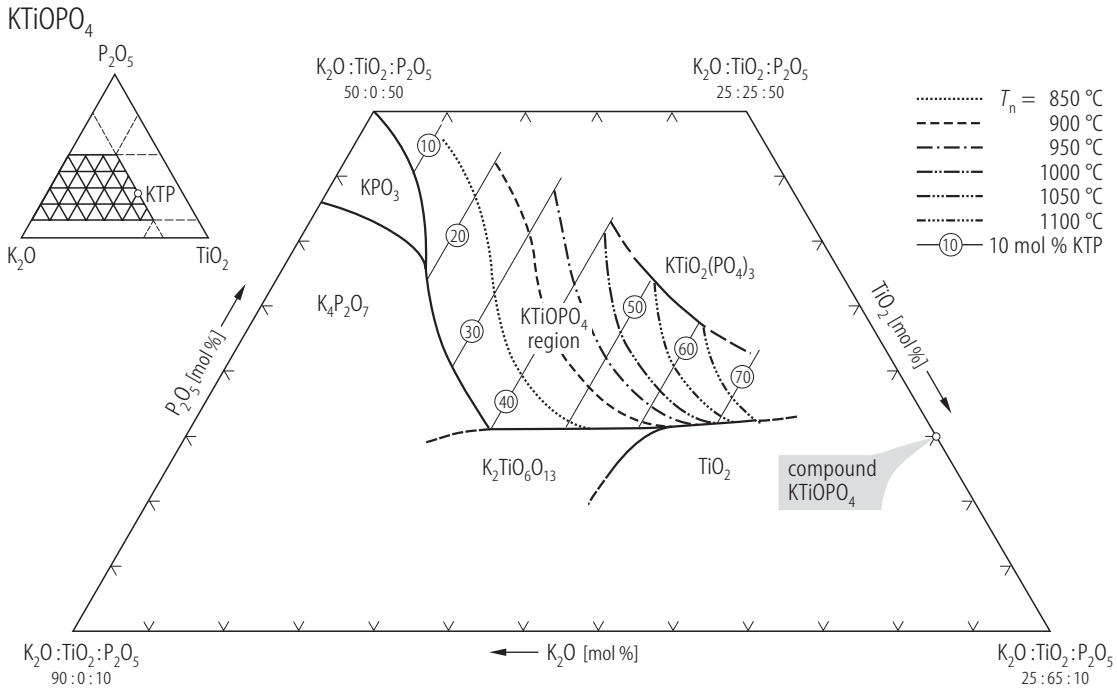

Fig. 35A-6-001. $KTiOPO_4$. Concentration region and spontaneous crystallization temperature of $KTiOPO_4$ in solvents of the K_2O–P_2O_5 system [90Ili2]. T_n: temperature of spontaneous crystallization.

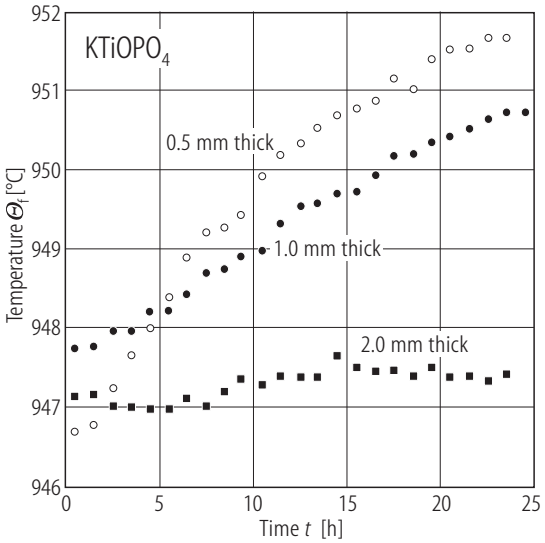

Fig. 35A-6-002. $KTiOPO_4$. Θ_f vs. t [91Bor]. Θ_f: transition temperature determined by the peak of κ_c at 1 MHz. t: the time for which the sample had been kept near Θ_f. Sample: flux grown crystals. The experiment was done in $60 \cdot 10^3$ m^3/h dry oxygen flowing condition. Parameter: sample thickness.

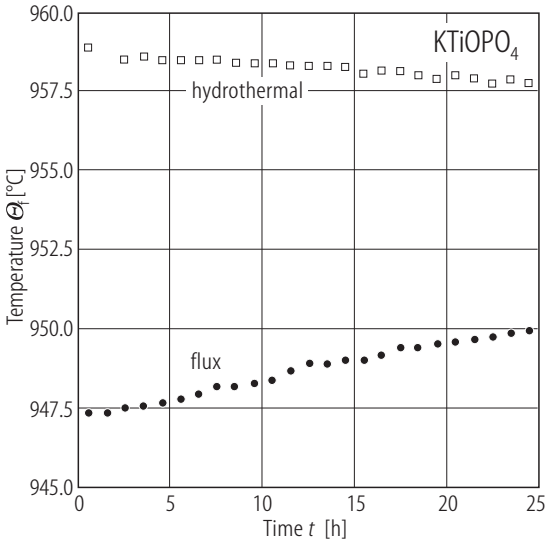

Fig. 35A-6-003. $KTiOPO_4$. Θ_f vs. t [91Bor]. Θ_f: transition temperature determined by the peak of κ_c at 1 MHz. t: the time for which the sample had been kept near Θ_f. Samples: flux and hydrothermally grown crystals. The experiment was done in $60 \cdot 10^3$ m^3/h dry oxygen flowing condition. Sample thickness: 1 mm.

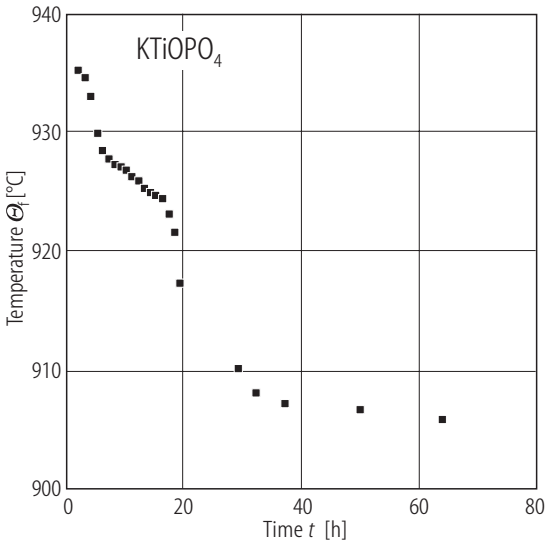

Fig. 35A-6-004. $KTiOPO_4$. Θ_f vs. t [95Ang]. t: annealing time at 970 °C. Sample: 1.0 mm thick crystal grown from self-flux.

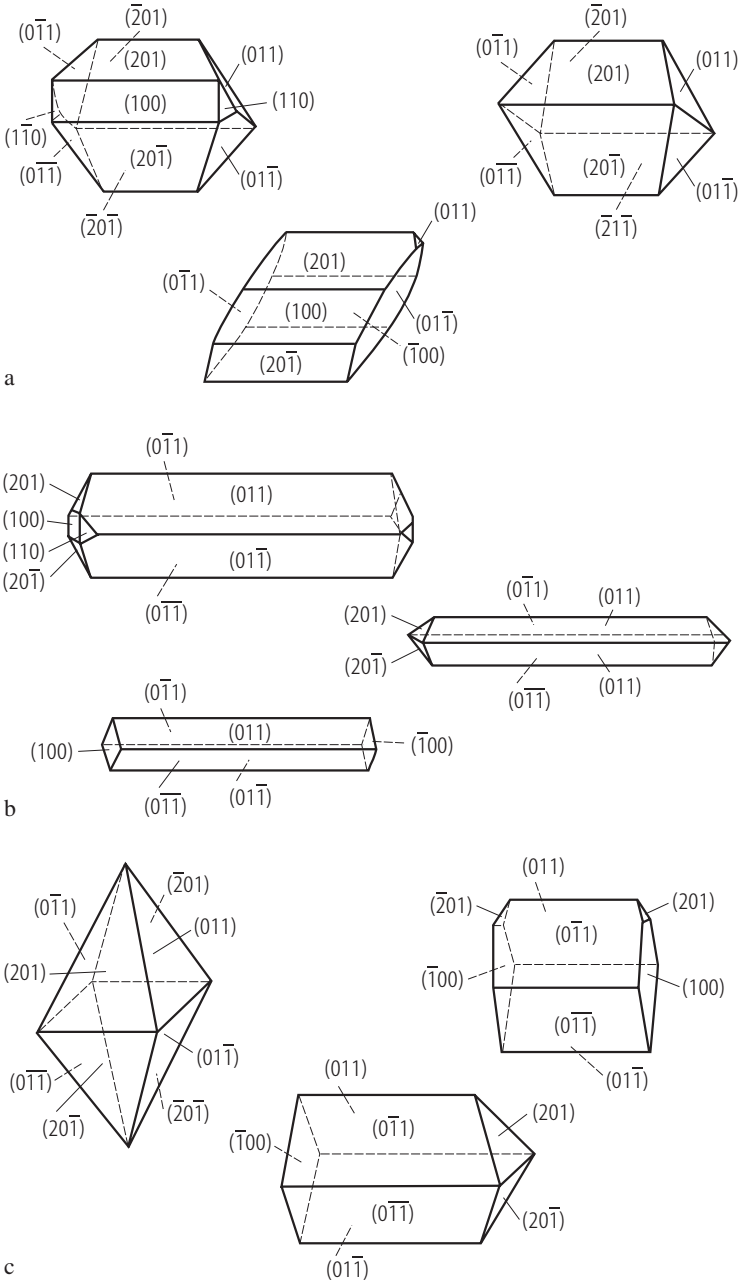

Fig. 35A-6-005. $KTiOPO_4$. Crystal habits obtained by flux method [86Pav]. (**a**) Crystals obtained from solutions of medium concentrations with slow cooling rates. (**b**) In conditions of high super-saturation. (**c**) From solutions of low concentrations.

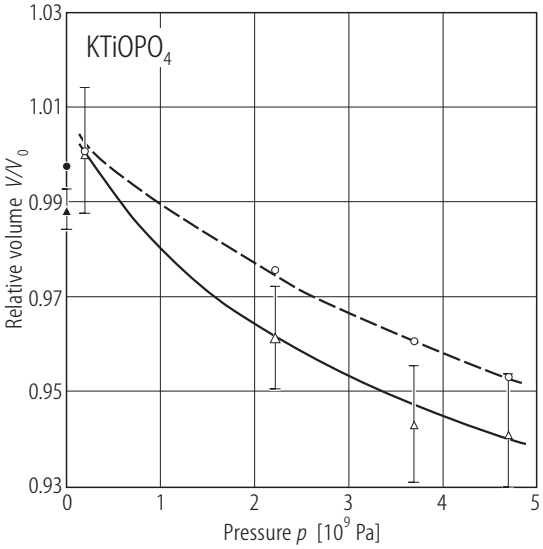

Fig. 35A-6-006. $KTiOPO_4$. The relative volume (V/V_0) of the unit-cell volume (open circle) and K cages (open triangle) (the K1 and K2 cages averaged) as a function of pressure, referred to the value V_0 at 0.2 GPa [92All]. The atmospheric-pressure values, shown as full circle and full triangle, are from [90Tho]. Note that the errors are smaller than the circular symbols when the error bars are not shown. The broken and full curves are from Murnagham fit to the relative volumes of the unit cell and the K cages, respectively.

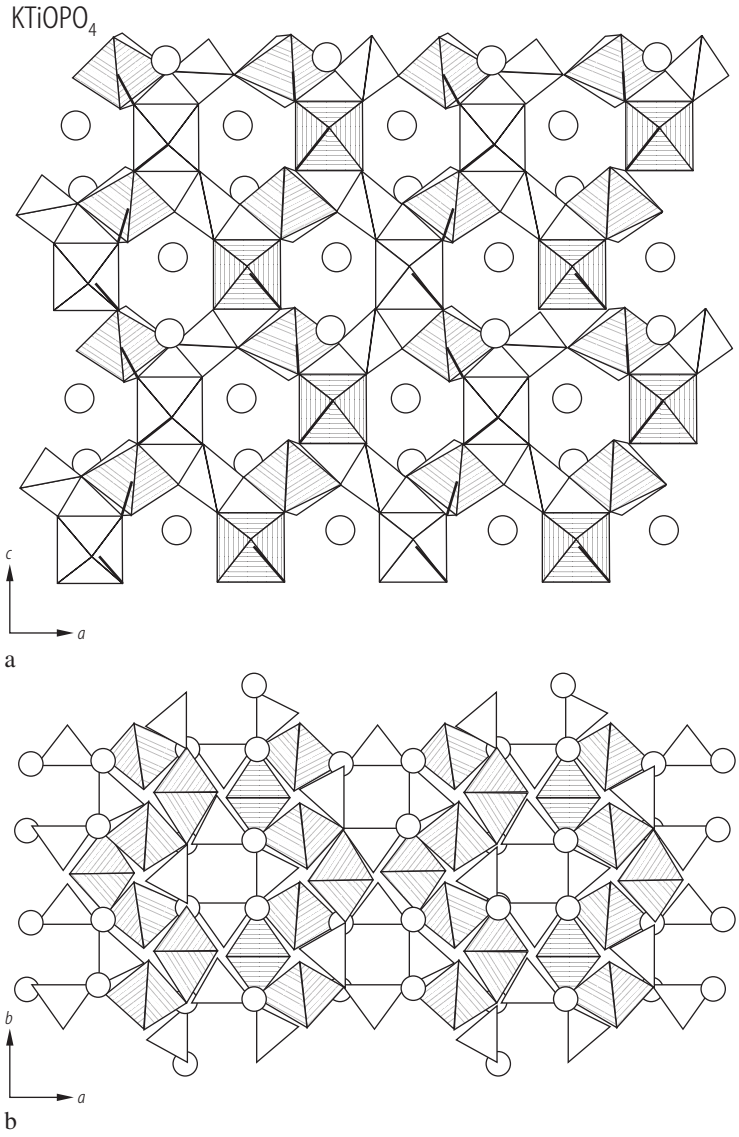

Fig. 35A-6-007. $KTiOPO_4$. Crystal structure [89Bie]. (**a**) *a–c* projection; (**b**) *a–b* projection. Shaded elements are the Ti octahedra, open elements are the P tetrahedra, and open circles are K atoms. The short Ti–O bonds are shown as bold lines.

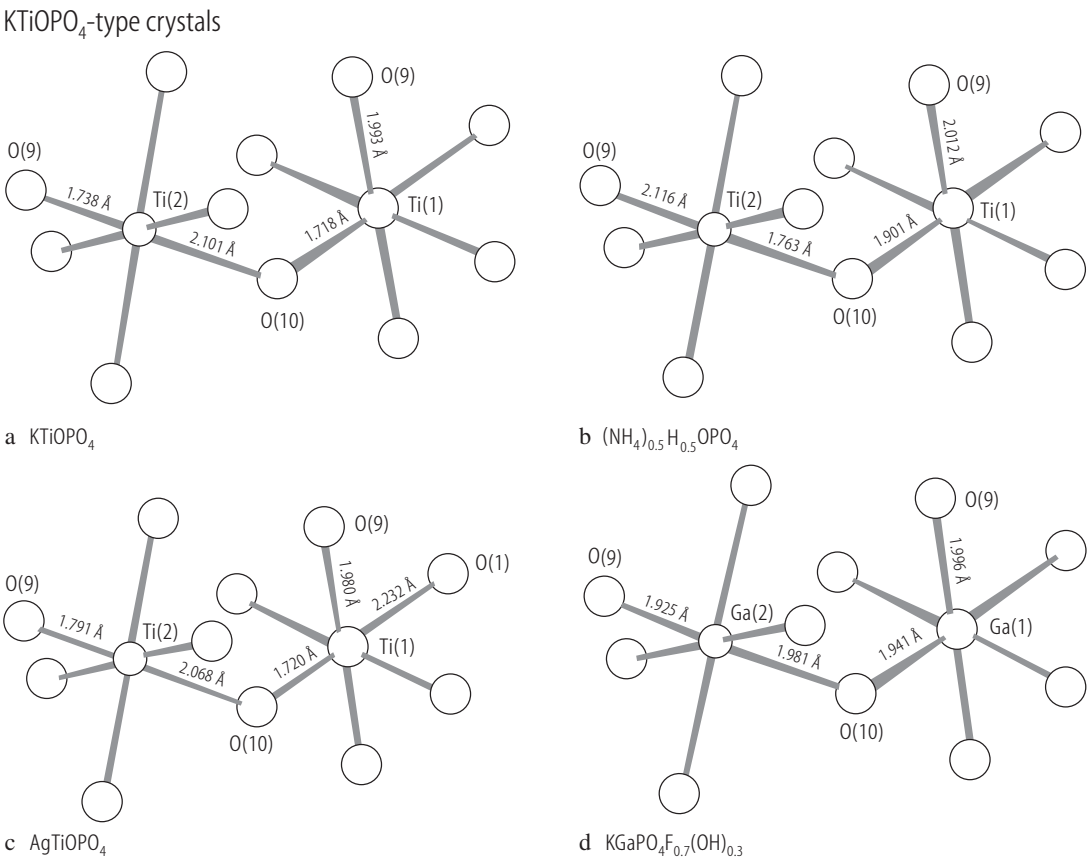

Fig. 35A-6-008. $KTiOPO_4$-type crystals. Two TiO_6 octahedra [89Phi]. (**a**) $KTiOPO_4$; (**b**) $(NH_4)_{0.5}H_{0.5}OPO_4$; (**c**) $AgTiOPO_4$; (**d**) $KGaPO_4F_{0.7}(OH)_{0.3}$.

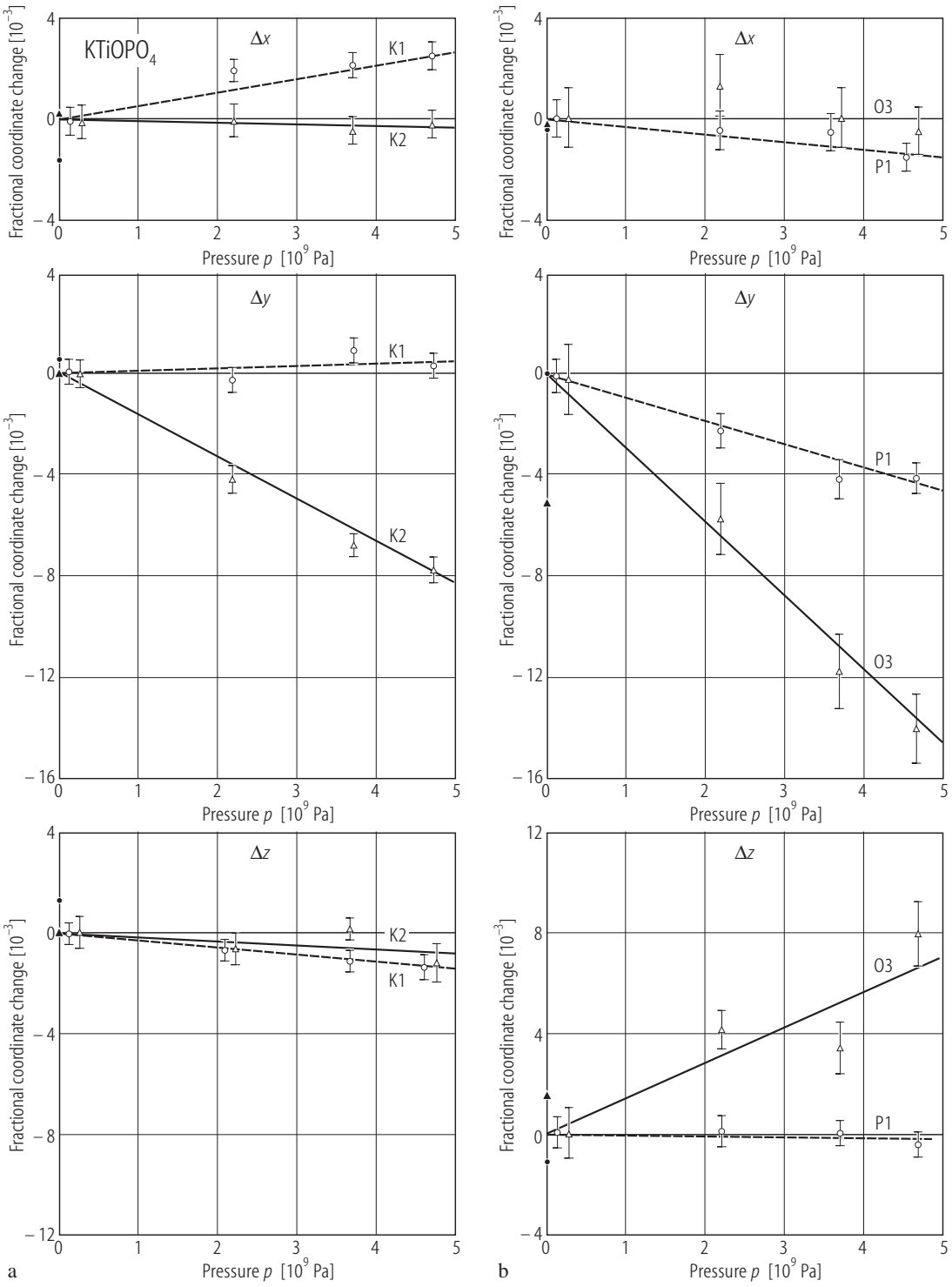

Fig. 35A-6-009. $KTiOPO_4$. (**a**) Fractional coordinate changes for the K1 (open circle) and K2 (open triangle) atoms, and (**b**) for the P1 (open circle) and O3 (open triangle) atoms relative to the 0.2 GPa values [92All]. The atmospheric-pressure values, shown as full circle and full triangle, are from [90Tho]. Note that some of the points have been translated slightly along the pressure axis to avoid overlap. The broken and full lines are a guide to the eye only.

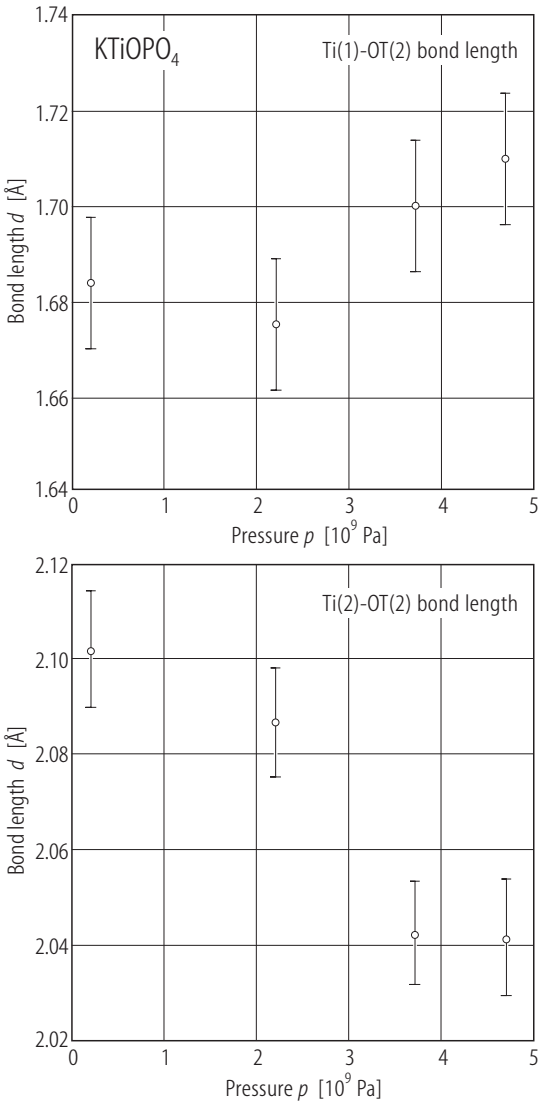

Fig. 35A-6-010. $KTiOPO_4$. *d* vs. *p* [91All]. *d*: Ti(1) – OT(2) or Ti(2) – OT(2) bond length. OT(2): oxygen of Ti(2) side.

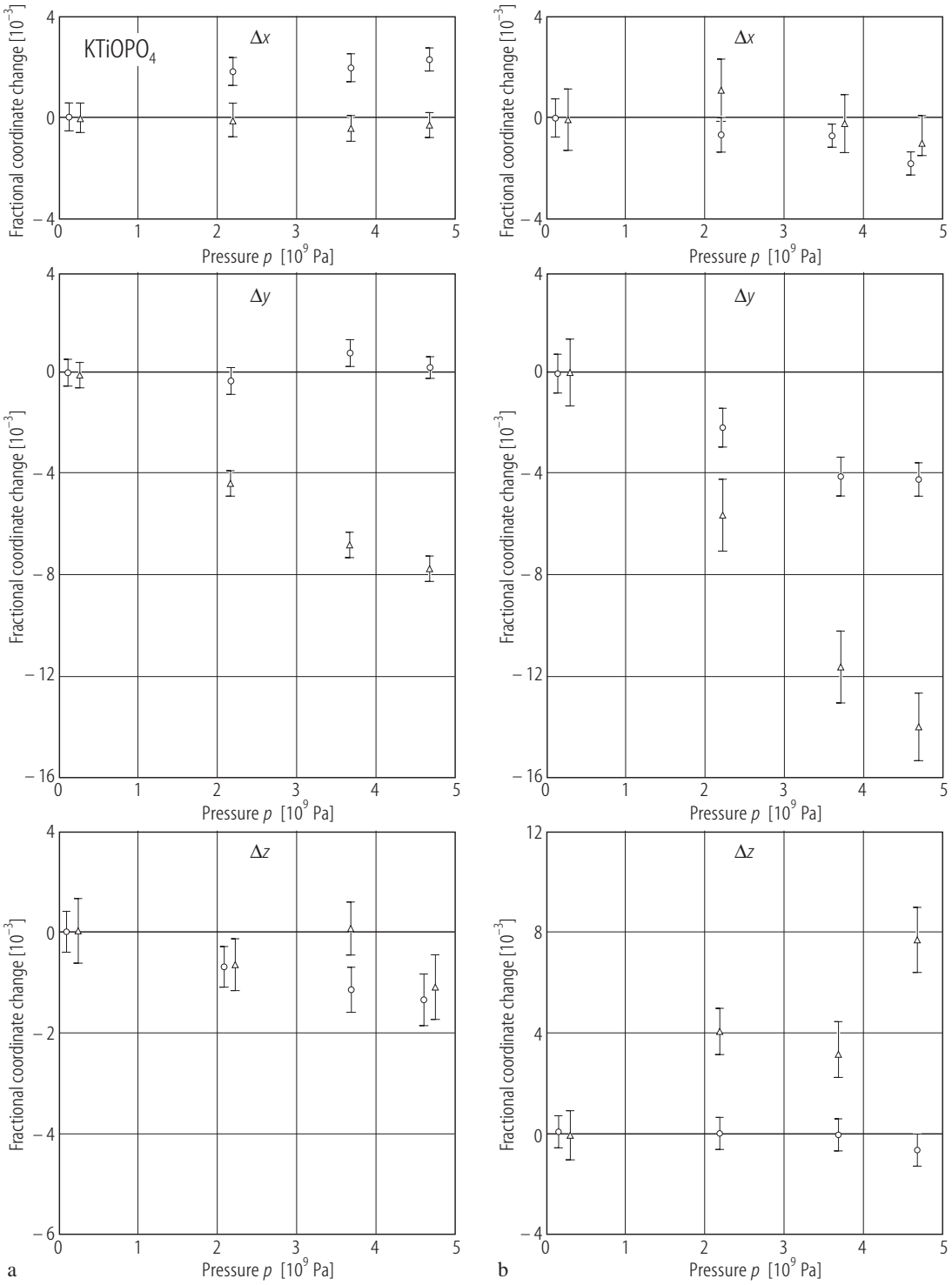

Fig. 35A-6-011. $KTiOPO_4$. Δx, Δy, Δz vs. p [91All]. Δx, Δy, Δz: fractional coordinate changes. (**a**) Open circle: K(1); open triangle: K(2); (**b**) open circle: P(1); open triangle: O(3). Some of the points were translated slightly along the pressure axis to avoid overlapping.

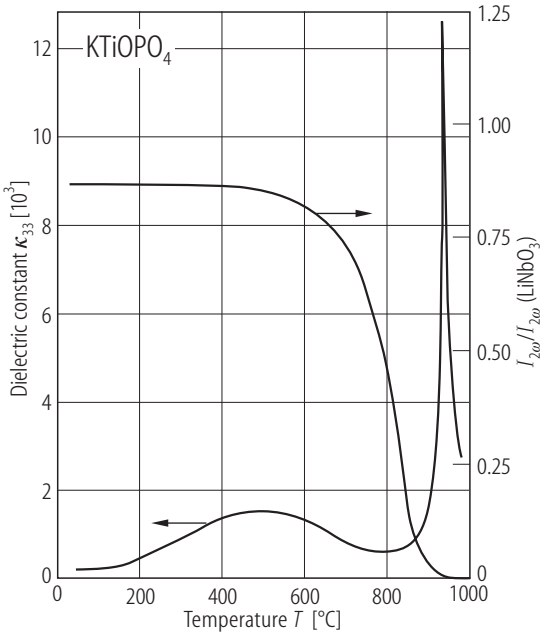

Fig. 35A-6-012. $KTiOPO_4$. κ_{33} , $I_{2\omega}/I_{2\omega}(LiNbO_3)$ vs. T [88Vor]. $I_{2\omega}/I_{2\omega}(LiNbO_3)$: intensity of the second harmonic generation compared to that of $LiNbO_3$. $\lambda = 1064$ nm.

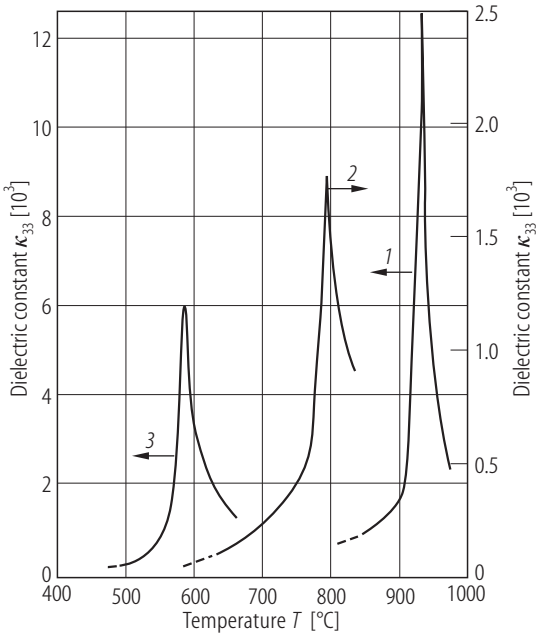

Fig. 35A-6-013. $KTiOPO_4$ (*1*) , $RbTiOPO_4$ (*2*), $TlTiOPO_4$ (*3*). κ_{33} vs. T [85Yan]. $f = 1$ MHz.

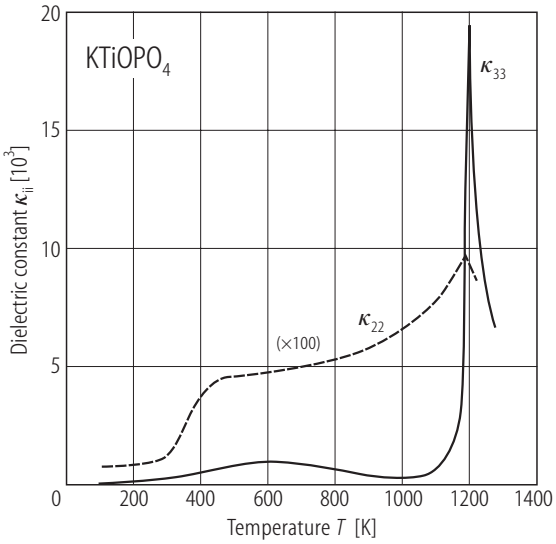

Fig. 35A-6-014. $KTiOPO_4$. κ_{33}, κ_{22} vs. T [91Ant]. f = 1 MHz.

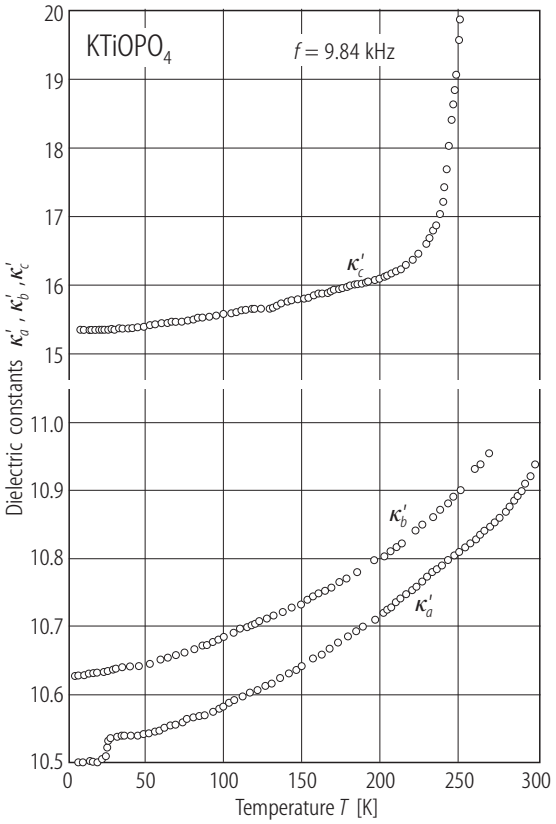

Fig. 35A-6-015. $KTiOPO_4$. κ'_a, κ'_b, κ'_c vs. T [89Pis]. f = 9.84 kHz.

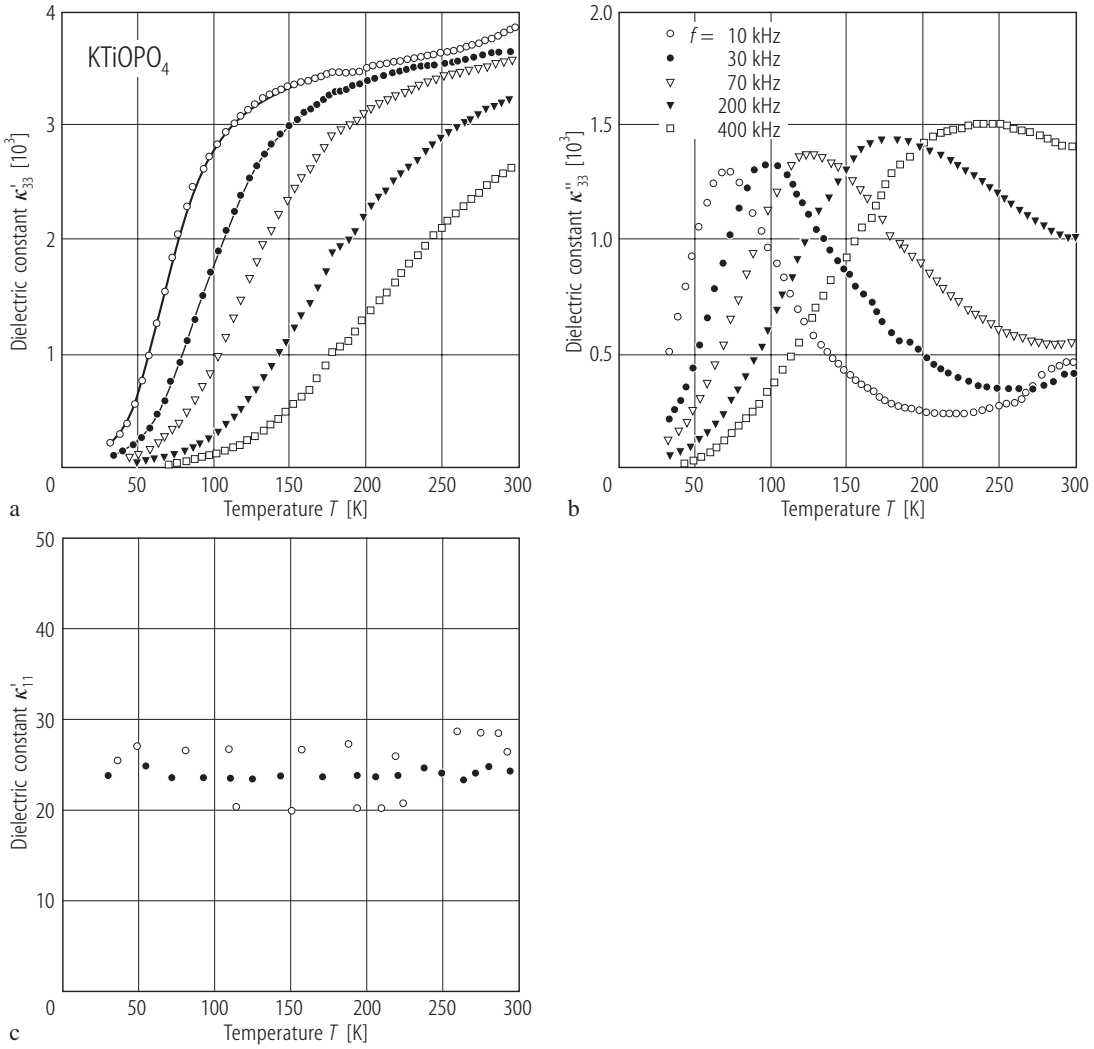

Fig. 35A-6-016. $KTiOPO_4$. κ'_{33}, κ''_{33}, κ'_{11} vs. T [94Cho]. (**a**) κ'_{33}, (**b**) κ''_{33}, (**c**) κ'_{11}. Parameter: f.

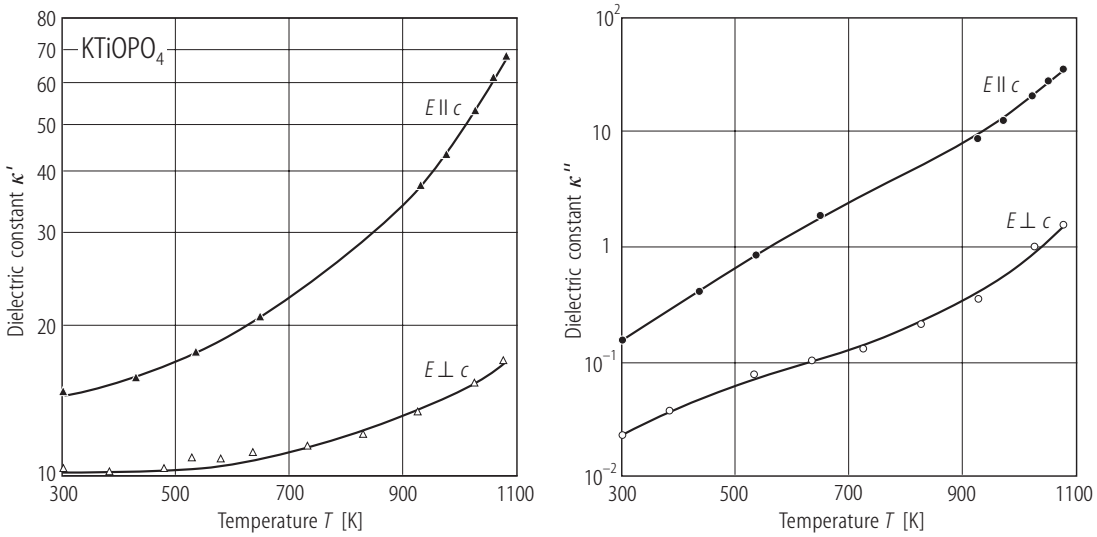

Fig. 35A-6-017. $KTiOPO_4$. Temperature dependences of κ' and κ'' at $f = 3 \cdot 10^{11}$ Hz. [90Vol]. The full symbols represent $E \parallel c$ and the open symbols represent $E \perp c$.

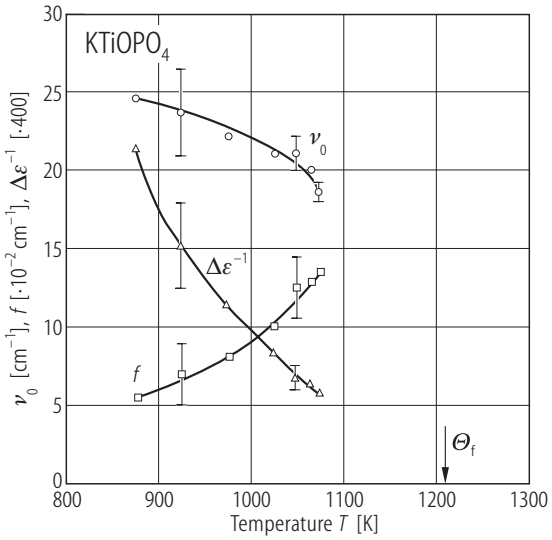

Fig. 35A-6-018. $KTiOPO_4$. Temperature dependences of the parameters of a submillimeter relaxator active in the $E \parallel c$ configuration [90Vol].

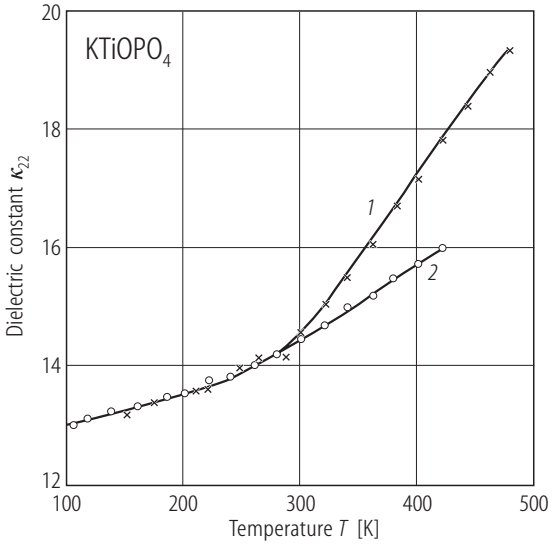

Fig. 35A-6-019. $KTiOPO_4$. κ_{22} vs. T [82Kal]. *1*: f = 800 MHz; *2*: f = 60 GHz.

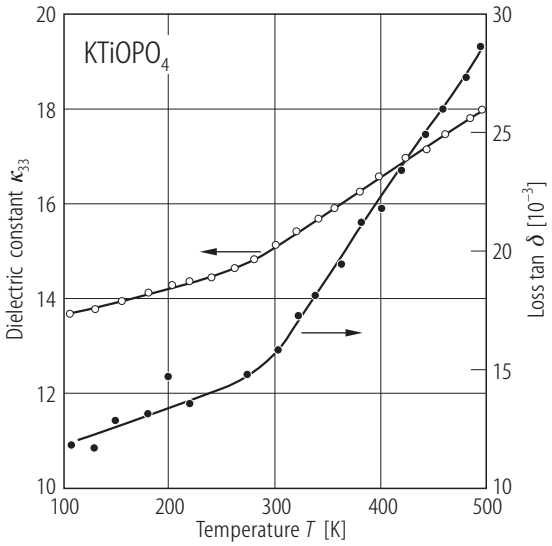

Fig. 35A-6-020. $KTiOPO_4$. κ_{33}, tan δ_{33} vs. T [82Kal]. f = 9 GHz.

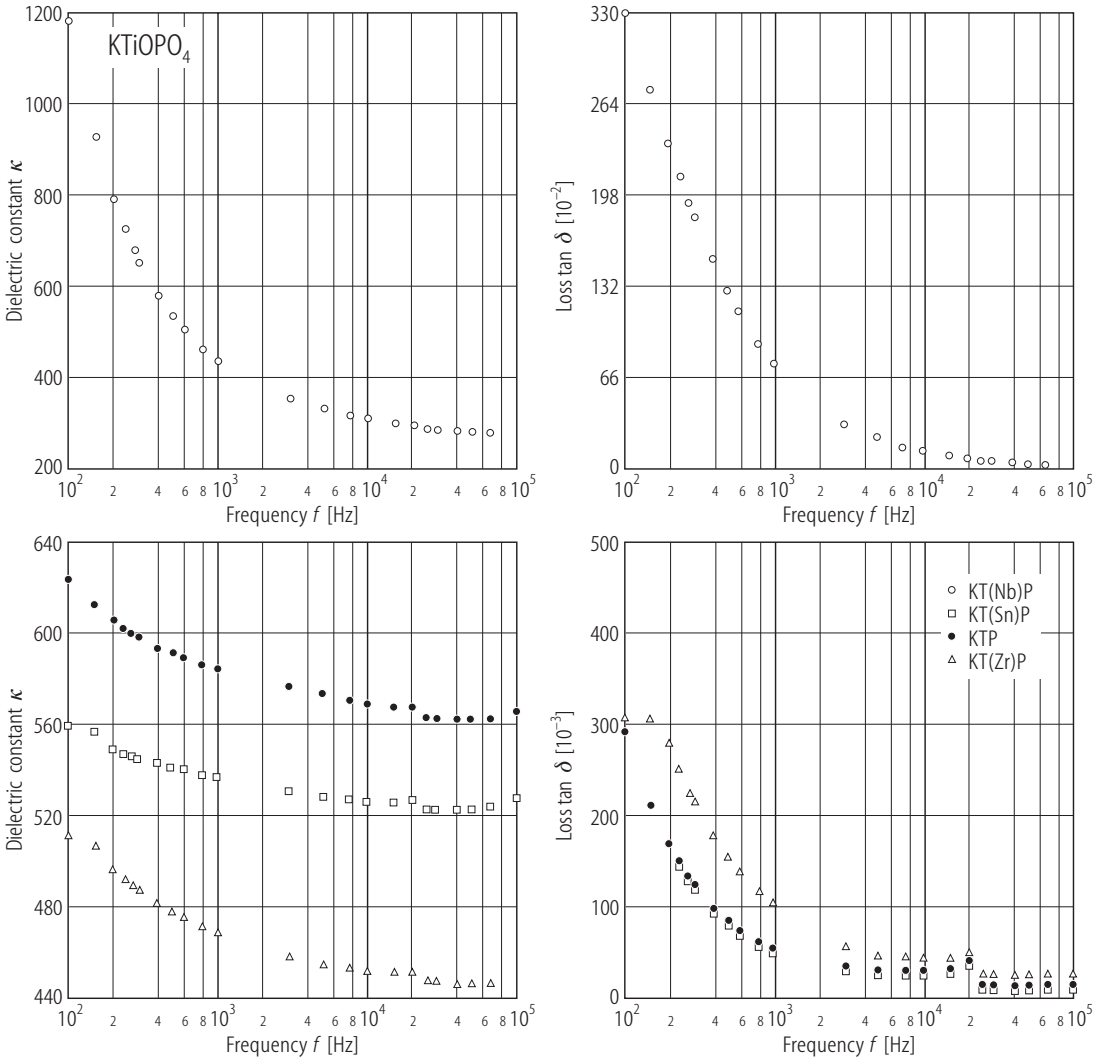

Fig. 35A-6-021. $KTiOPO_4$, $KTiOPO_4$:Nb (15 mol%), $KTiOPO_4$:Zr (15 mol%), $KTiOPO_4$:Sn (15 mol%). κ; tan δ vs. f [92Sas]. f: frequency. Powder samples.

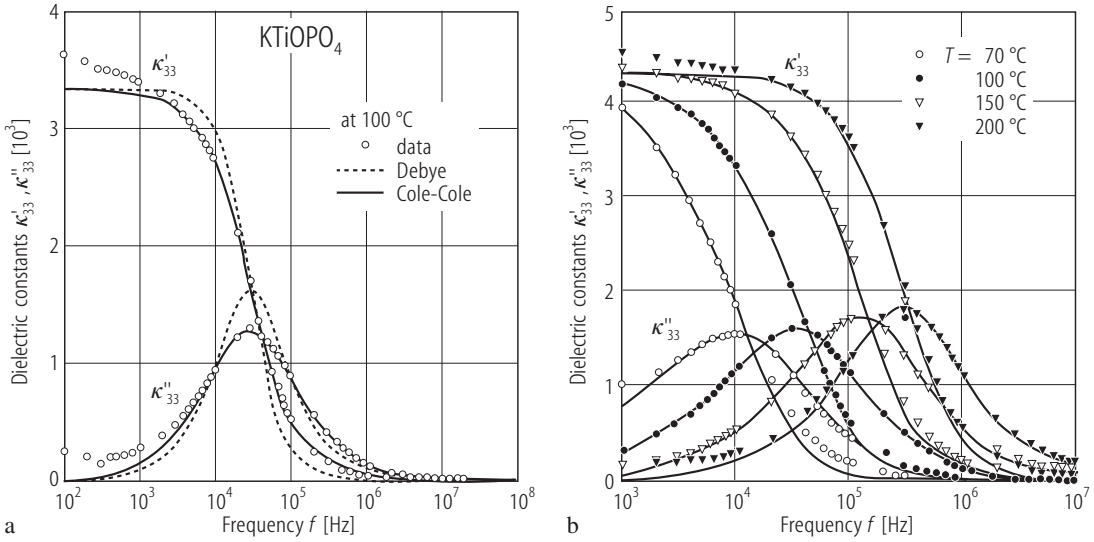

Fig. 35A-6-022. $KTiOPO_4$. κ'_{33}, κ''_{33} vs. f [94Cho]. Parameter: T. Dotted line: fitting curves for Debye monodispersive formula. Full line: fitting curve for Cole-Cole polydispersive curve.

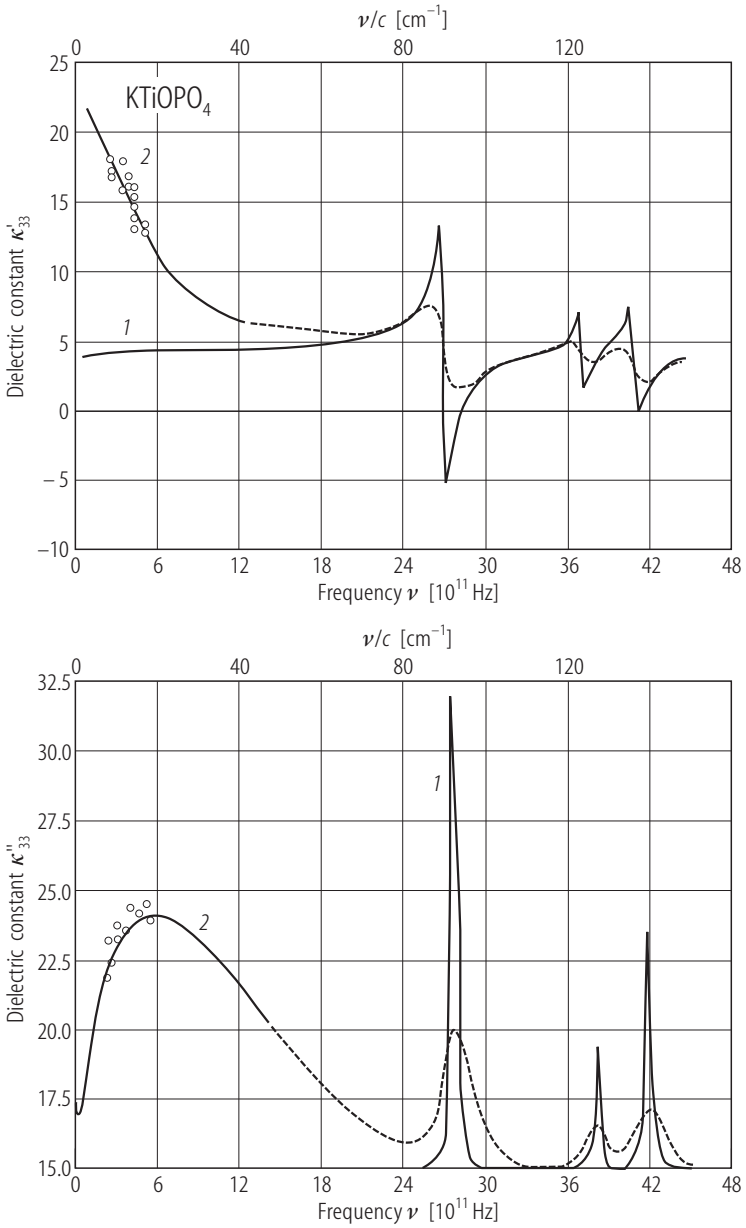

Fig. 35A-6-023. $KTiOPO_4$. Variation in the dielectric spectra due to a change in temperature from the room temperature value (*1*) to 1100 K (*2*) [90Vol].

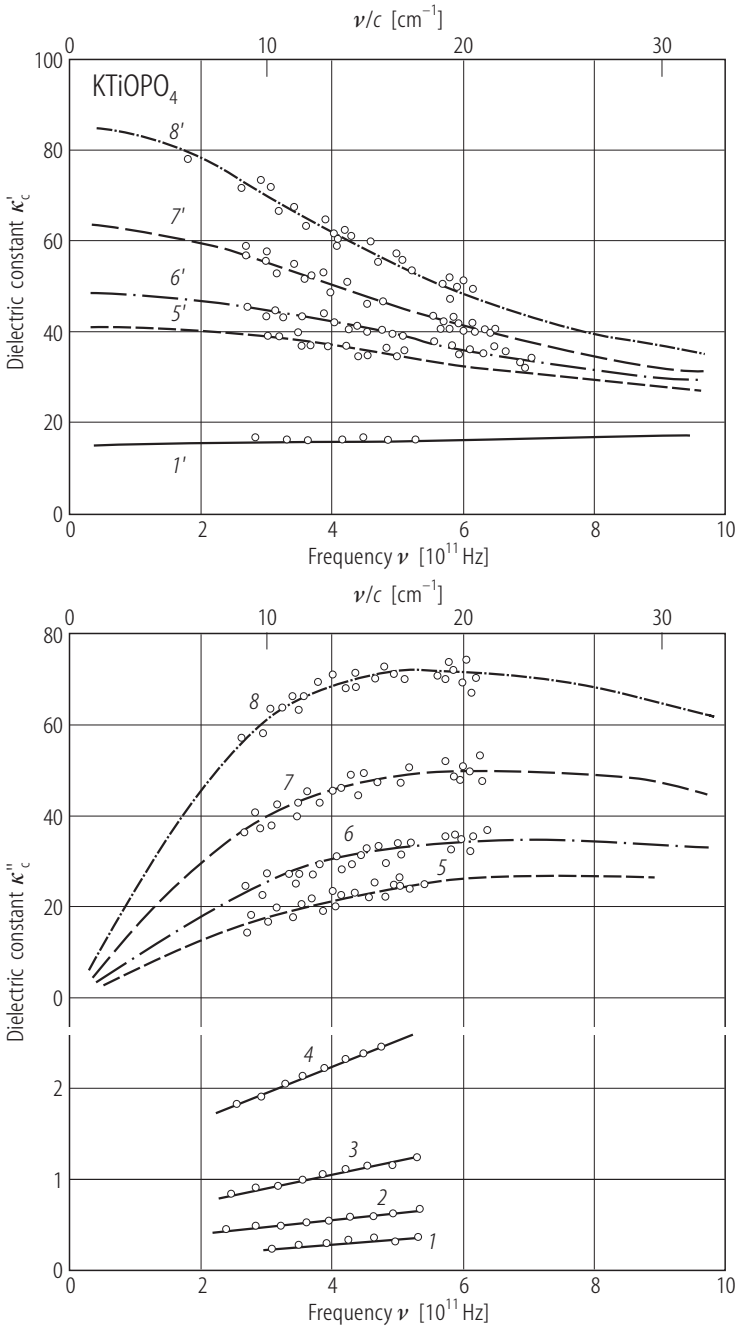

Fig. 35A-6-024. $KTiOPO_4$. κ_c', κ_c'' vs. ν in the submillimeter region [90Vol]. Parameter: *T*. *1*), *1′*) T = 295 K; *2*) 425 K; *3*) 525 K; *4*) 640 K; *5*), *5′*) 925 K; *6*), *6′*) 975 K; *7*), *7′*) 1025 K; *8*), *8′*) 1075 K. Curves *5*–*8* and *5′*–*8′* are calculated using a relaxation model of the dispersion.

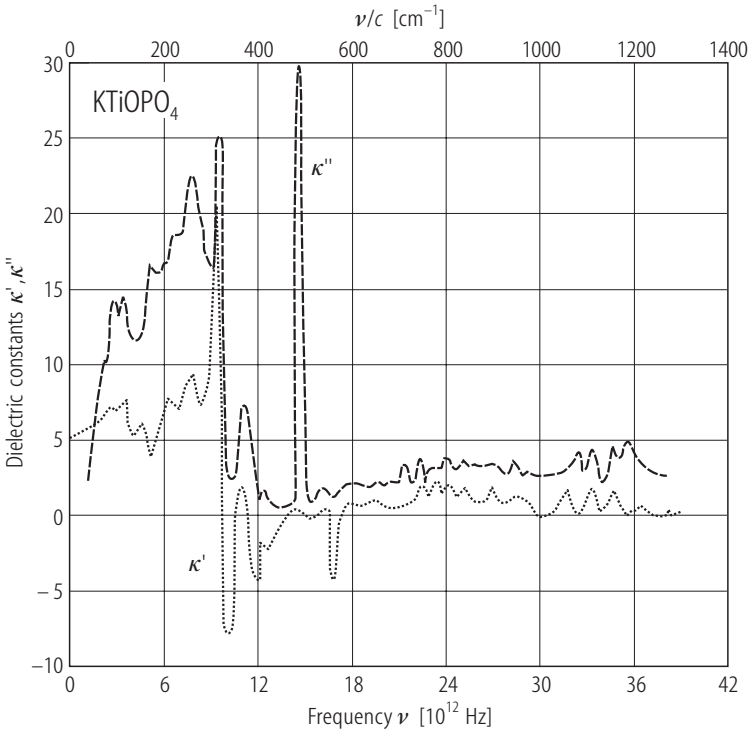

Fig. 35A-6-025. $KTiOPO_4$. κ', κ'' vs. ν [89Dov1].

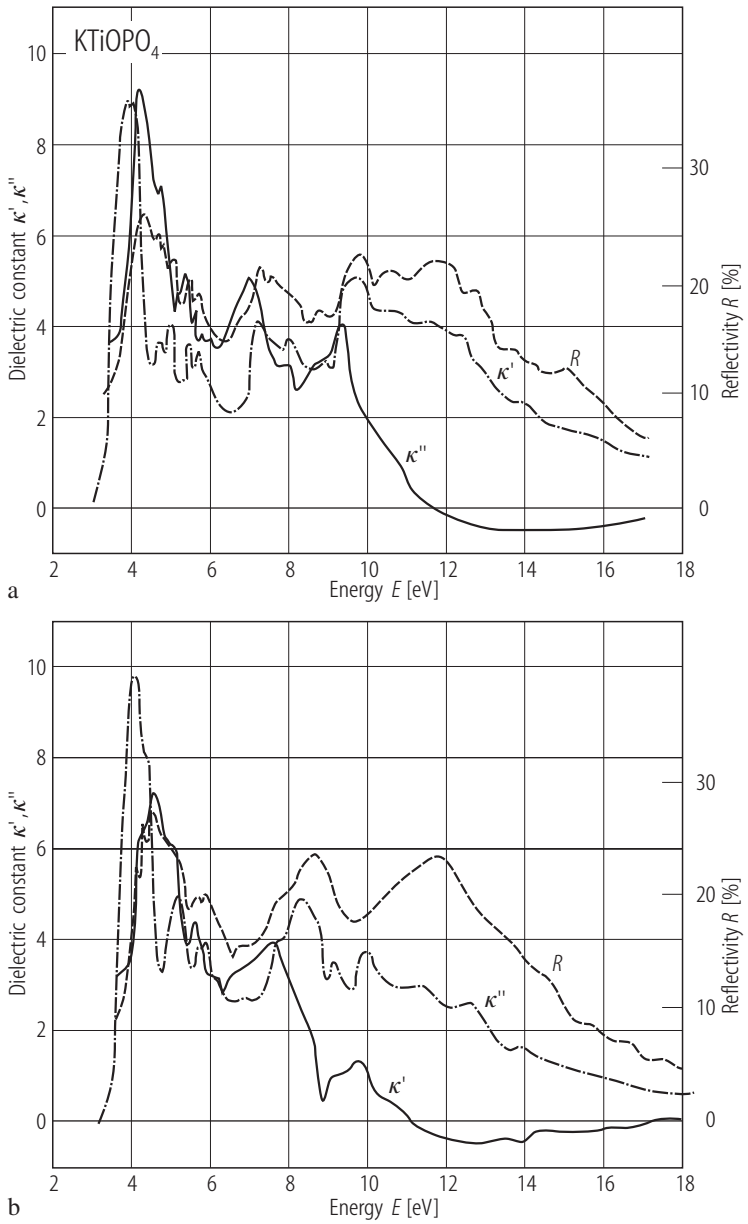

Fig. 35A-6-026. $KTiOPO_4$. R, κ', κ'' vs. E [89Dov2]. R: reflectivity of UV light. E: photon energy. (**a**) Polarization of light: x. (**b**) Polarization of light: z.

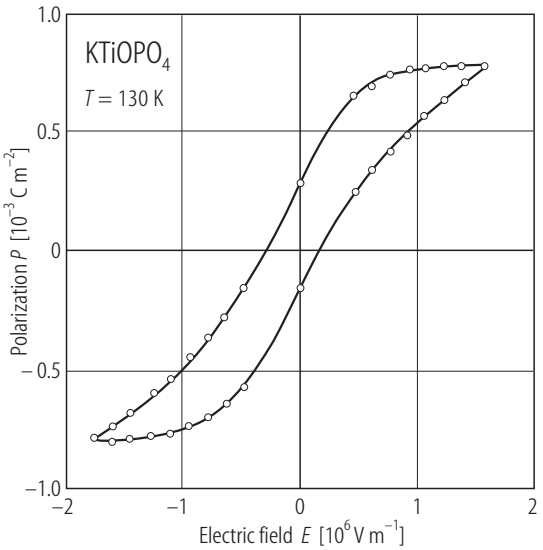

Fig. 35A-6-027. $KTiOPO_4$. P vs. E [90Sha]. P: electric polarization measured by charge integration method. T = 130 K. Evidence for ferroelectricity.

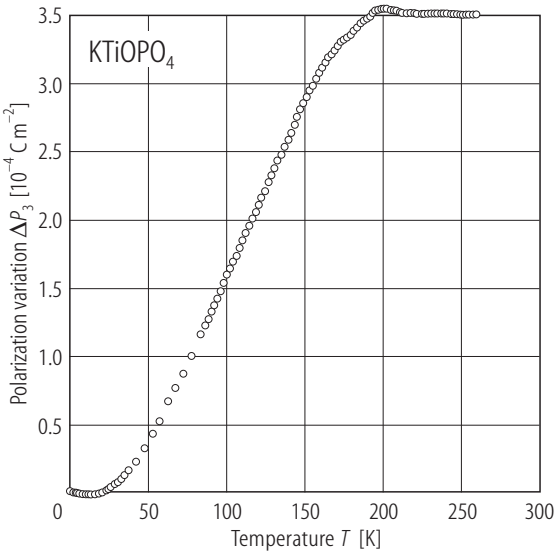

Fig. 35A-6-028. $KTiOPO_4$. ΔP_3 vs. T [90Sha]. ΔP_3: Variation in the spontaneous polarization.

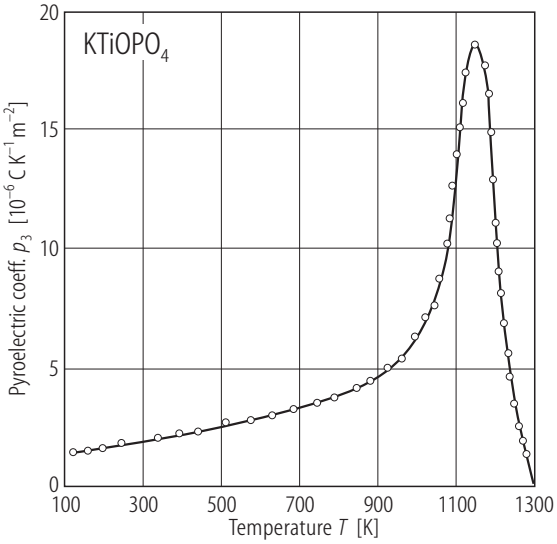

Fig. 35A-6-029. $KTiOPO_4$. p_3 vs. T [91Ant]. p_3: pyroelectric coefficient.

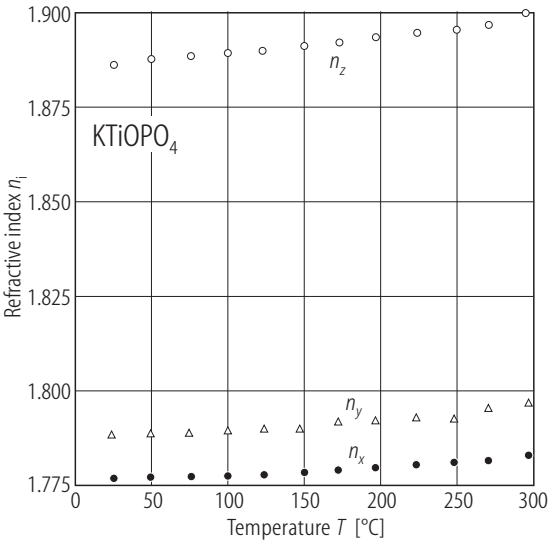

Fig. 35A-6-030. $KTiOPO_4$. n_x, n_y, n_z vs. T [76Zum]. n_x, n_y, n_z: refractive indices.

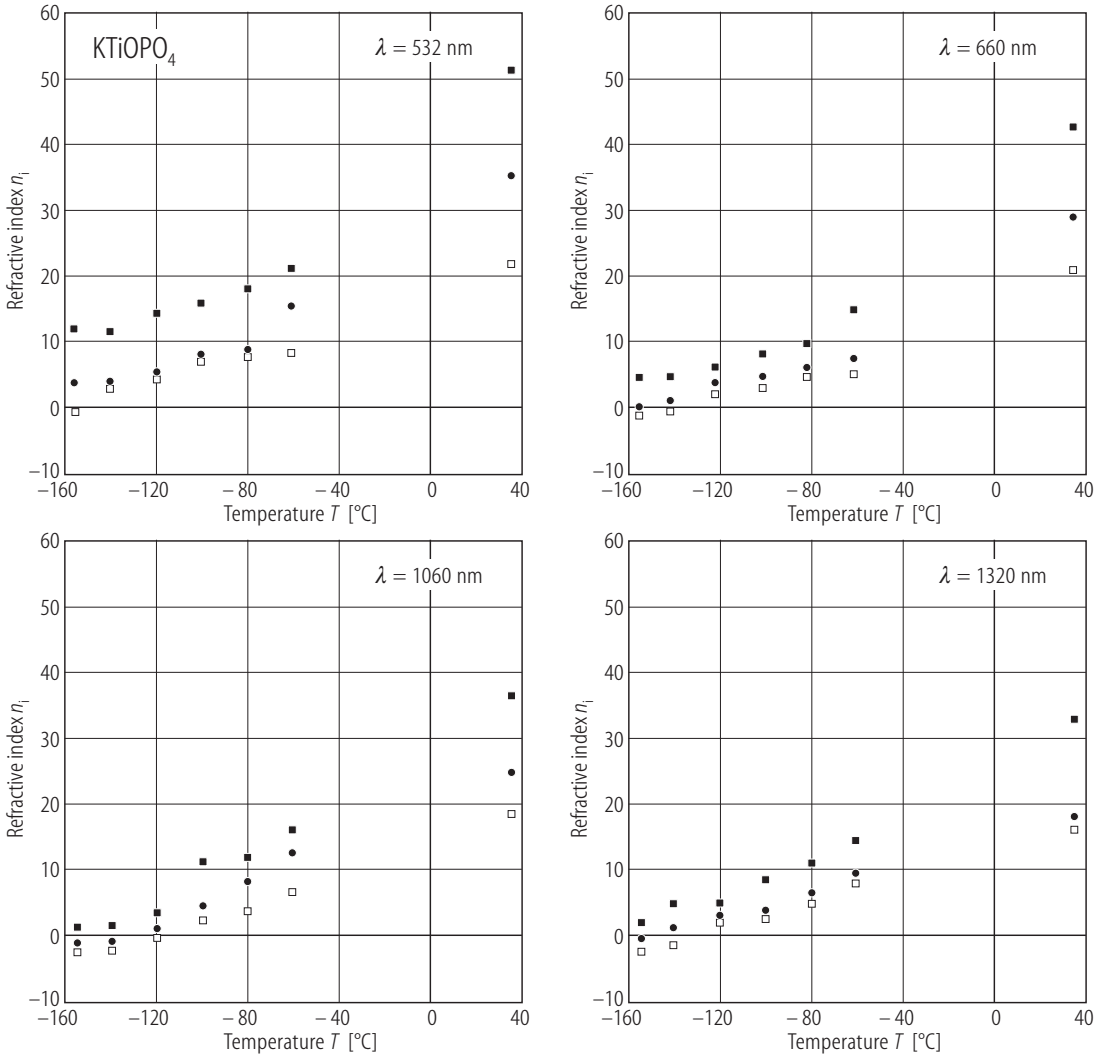

Fig. 35A-6-031. $KTiOPO_4$. n_x, n_y, n_z vs. T [88Get]. Parameter: λ. Open square: n_x, full circle: n_y, full square: n_z.

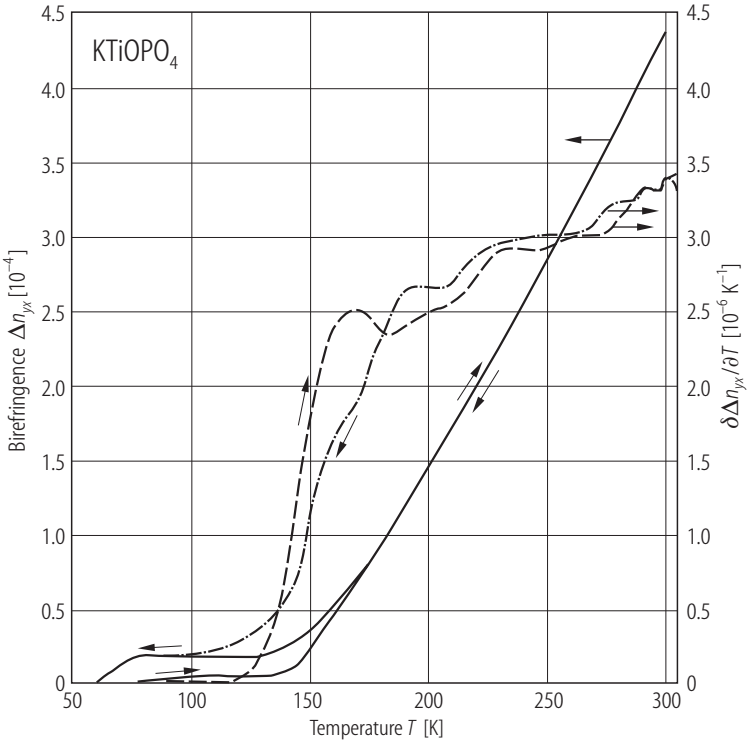

Fig. 35A-6-032. $KTiOPO_4$. Δn_{yx}, $\partial\Delta n_{yx}/\partial T$ vs. T [89Pis]. Δn_{yx}: birefringence. $\lambda = 632.8$ nm.

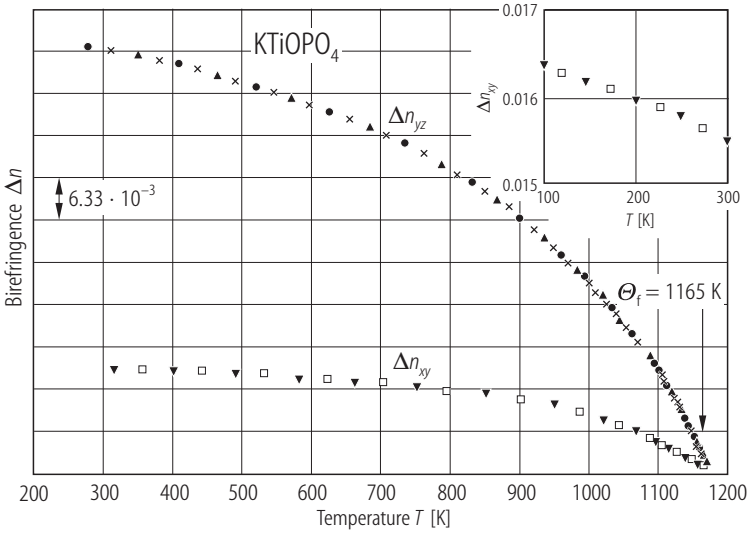

Fig. 35A-6-033. $KTiOPO_4$. Δn_{xy}, Δn_{yz} vs. T [90Sha]. Δn_{xy}, Δn_{yz}: spontaneous birefingences. $\lambda = 632.8$ nm.

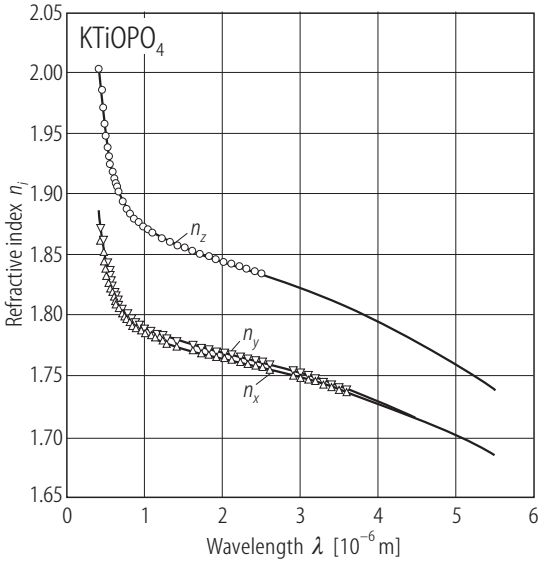

Fig. 35A-6-034. $KTiOPO_4$. n_x, n_y, n_z vs. λ [95Fen].

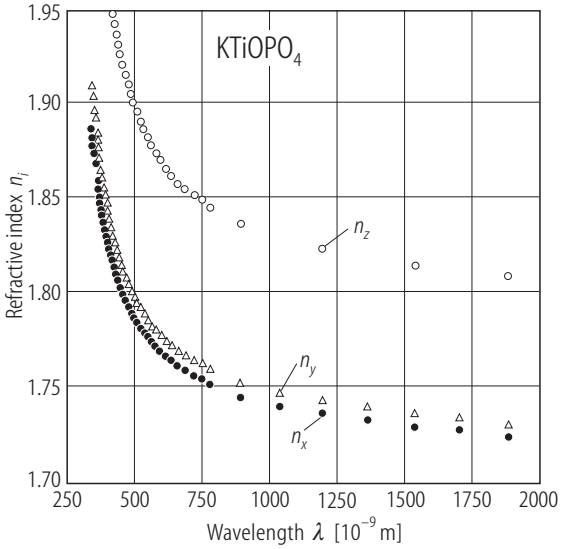

Fig. 35A-6-035. $KTiOPO_4$. n_x, n_y, n_z vs. λ [76Zum].

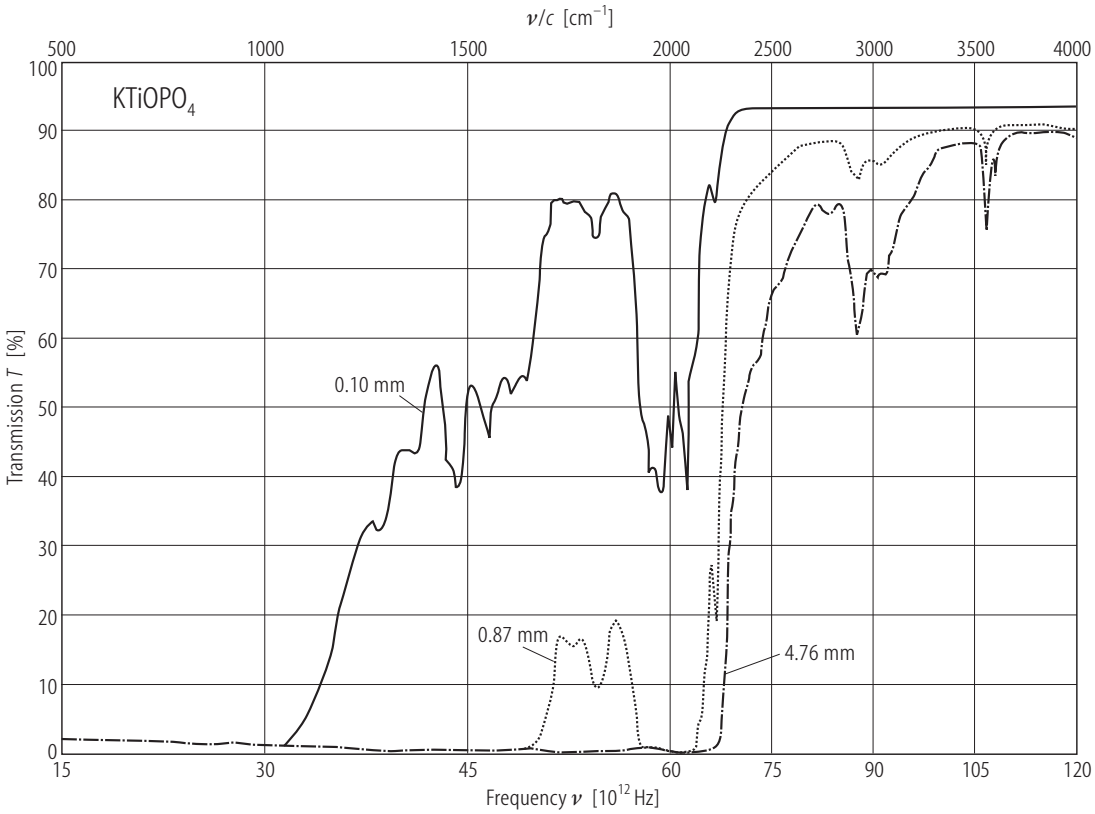

Fig. 35A-6-036. $KTiOPO_4$. T vs. ν [91Jac1]. T: transmission. Parameter: sample thickness.

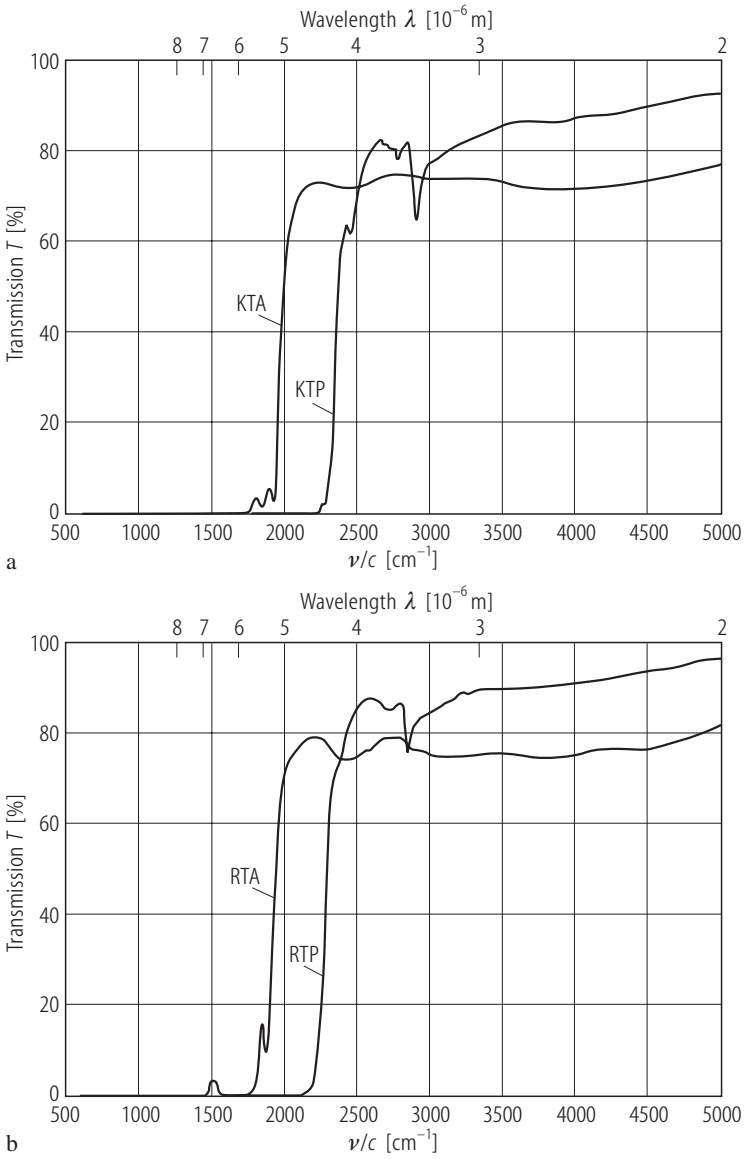

Fig. 35A-6-037. (**a**) $KTiOPO_4$, $KTiOAsO_4$, (**b**) $RbTiOPO_4$, $RbTiOAsO_4$. T vs. λ [91Che1]. T: optical transmission. Sample: 3 mm thick x-plate.

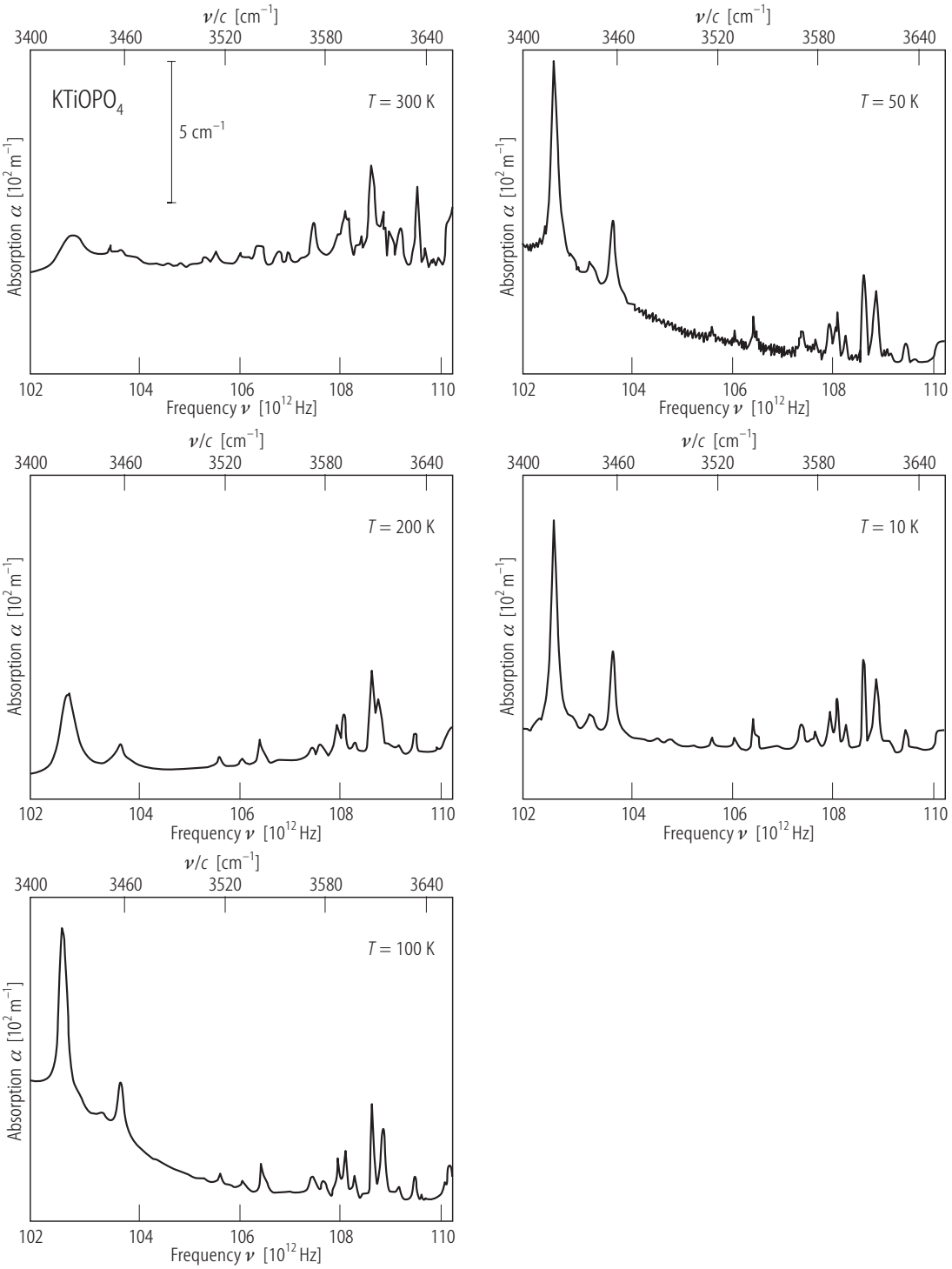

Fig. 35A-6-038. $KTiOPO_4$. α vs. ν [92Mor]. α: absorption coefficient of the infrared light. Sample: low-temperature hydrothermal grown crystal. Incident radiation propagation: *z*-direction. Parameter: *T*.

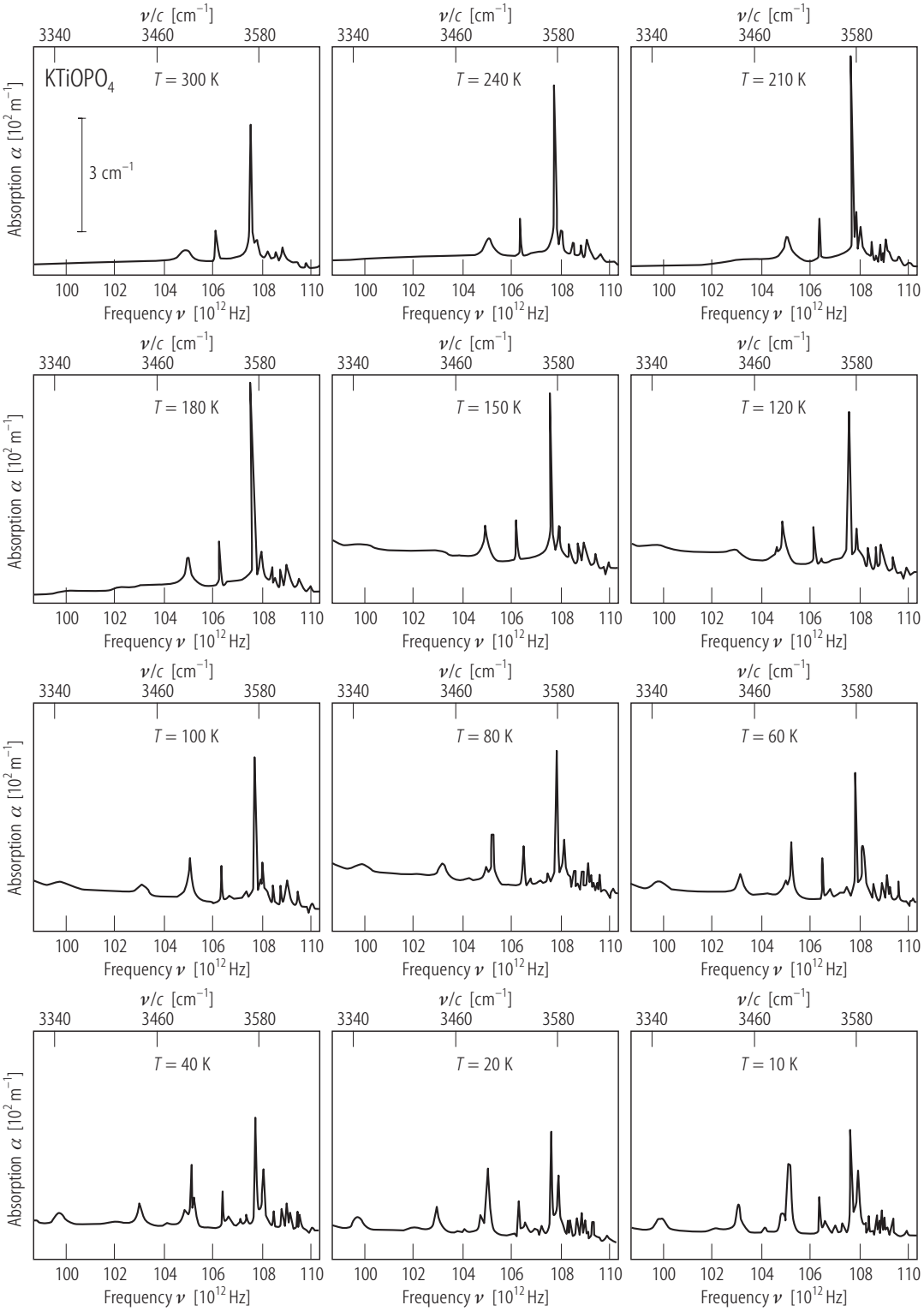

Fig. 35A-6-039. $KTiOPO_4$. α vs. ν [92Mor]. α: absorption coefficient of the infrared light. Sample: high-temperature hydrothermal grown crystal. Incident radiation propagation: *z*-direction. Parameter: *T*.

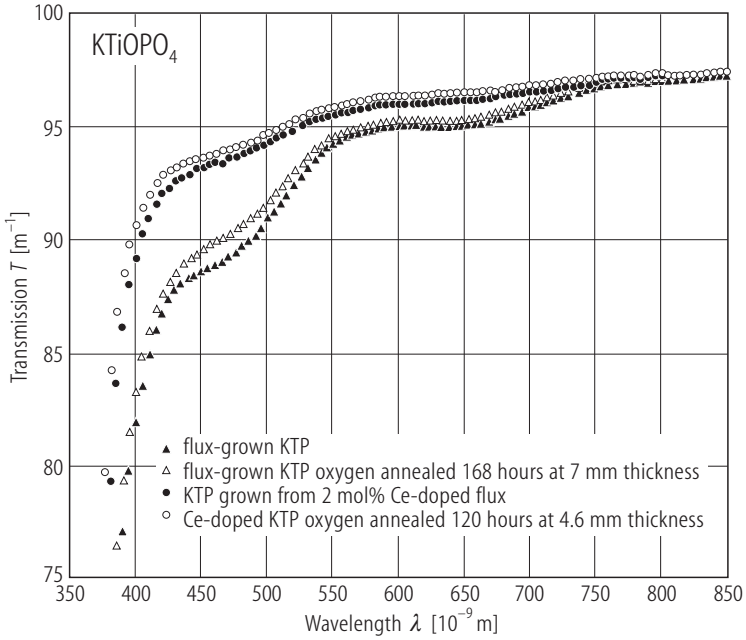

Fig. 35A-6-040. $KTiOPO_4$, $KTiOPO_4$:Ce. T vs. λ [92Bor]. T: optical transmission per meter.

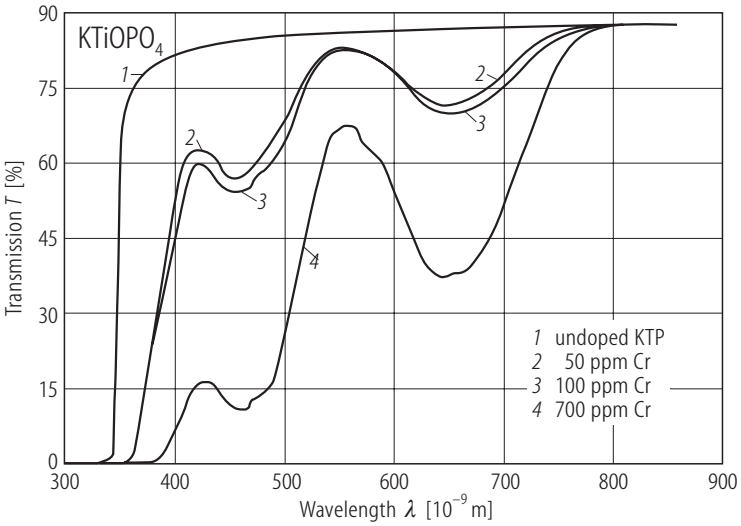

Fig. 35A-6-041. $KTiOPO_4$. T vs. λ [91McG]. T: optical transmission. Parameter: Cr doping concentration.

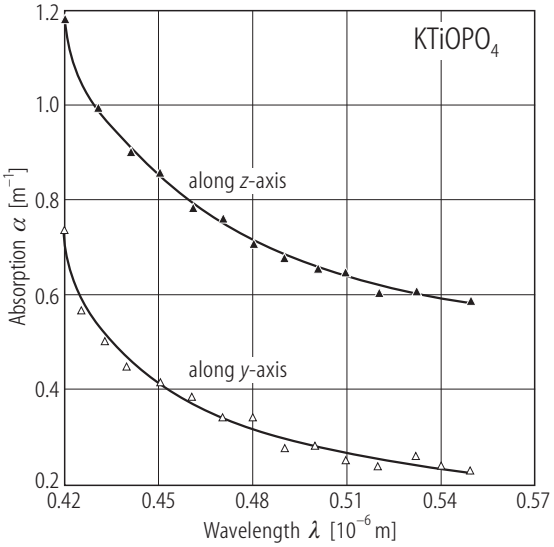

Fig. 35A-6-042. $KTiOPO_4$. α vs. λ [90Man]. α: optical absorption coefficient.

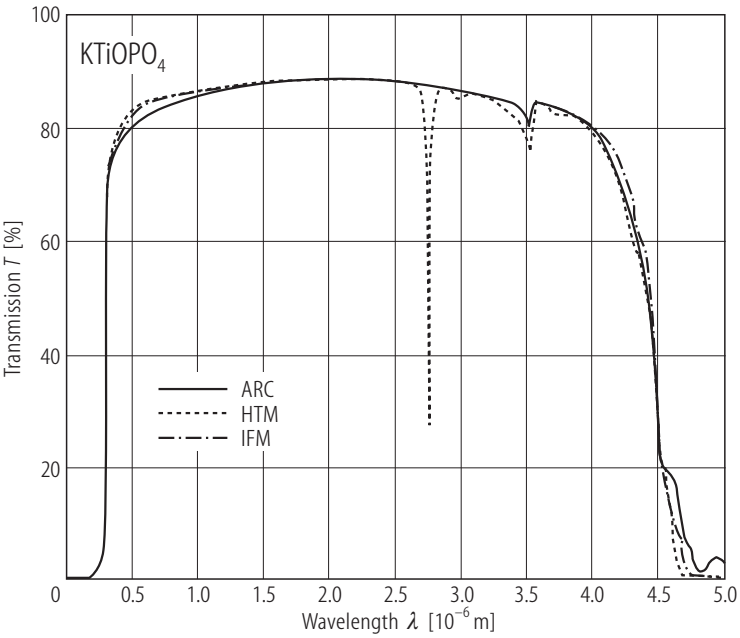

Fig. 35A-6-043. $KTiOPO_4$. T vs. λ [85She]. T: light transmission. HTM: hydrothermal method. ARC: accelerated crucible rotation. IFM: improved flux method.

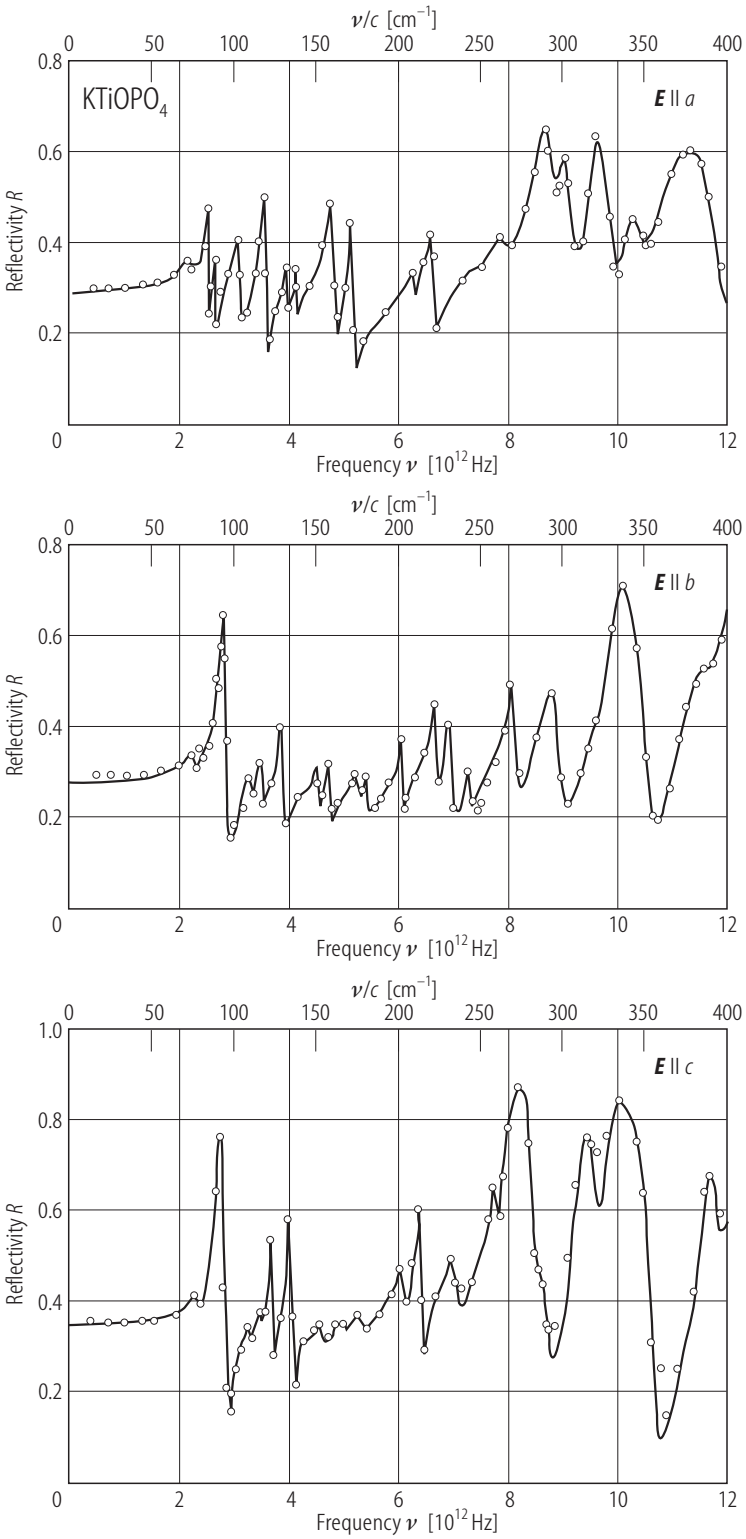

Fig. 35A-6-044. $KTiOPO_4$. R vs. ν [88Kug]. R: infrared reflectivity spectra. $T = 7$ K. The lines show calculated results.

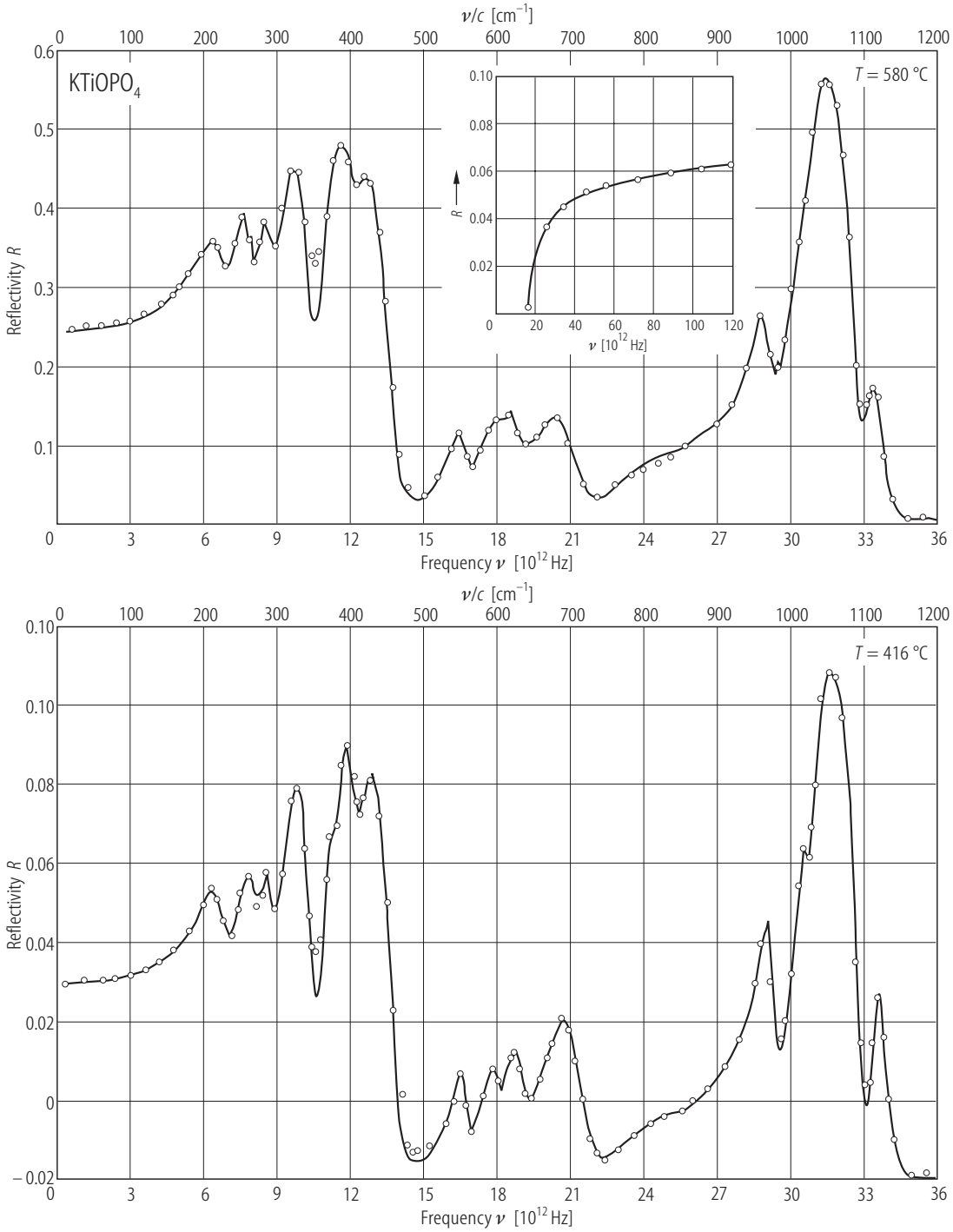

Fig. 35A-6-045. $KTiOPO_4$. R vs. ν [91Moh]. R: infrared reflectivity for B_1 symmetry species. Parameter: T. The lines show calculated results.

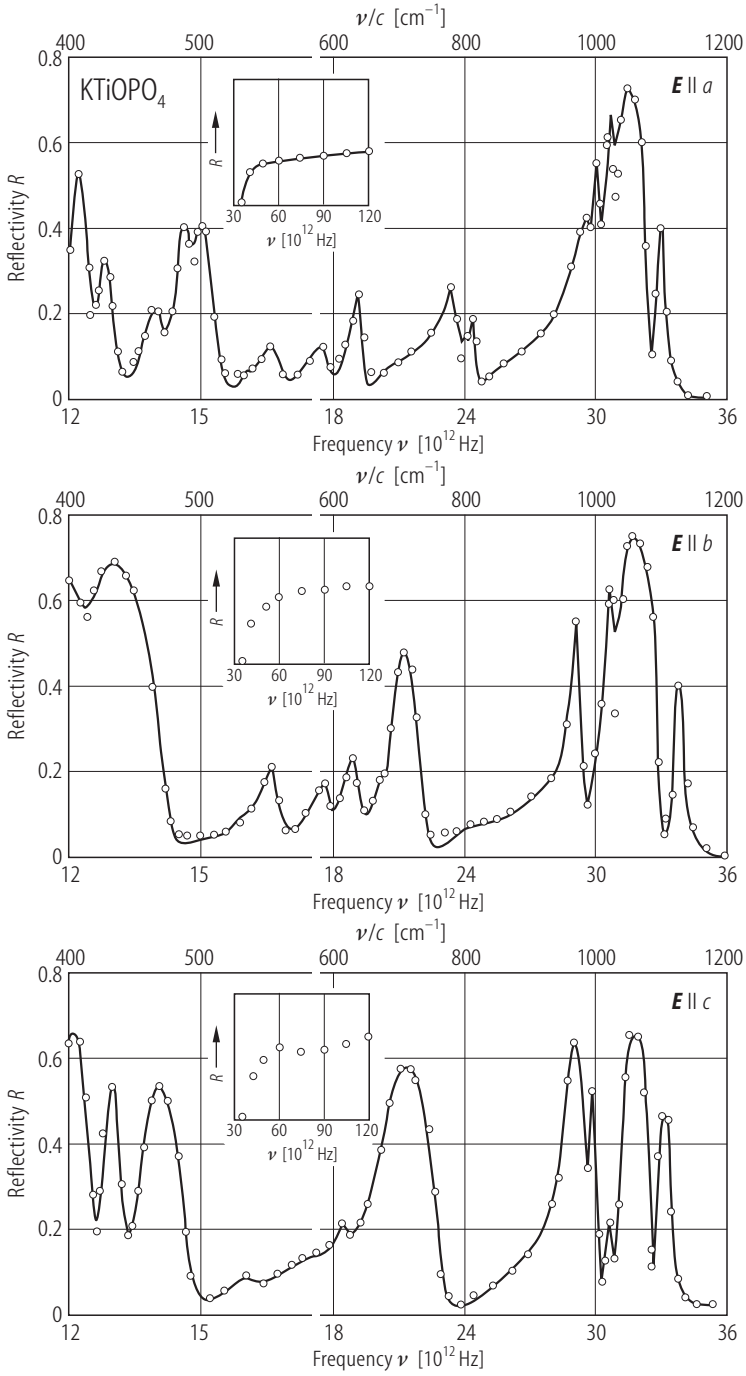

Fig. 35A-6-046. $KTiOPO_4$. R vs. ν [88Kug]. R: infrared reflectivity spectra. T = 300 K. The high-energy range is shown in the insets. The lines show calculated results.

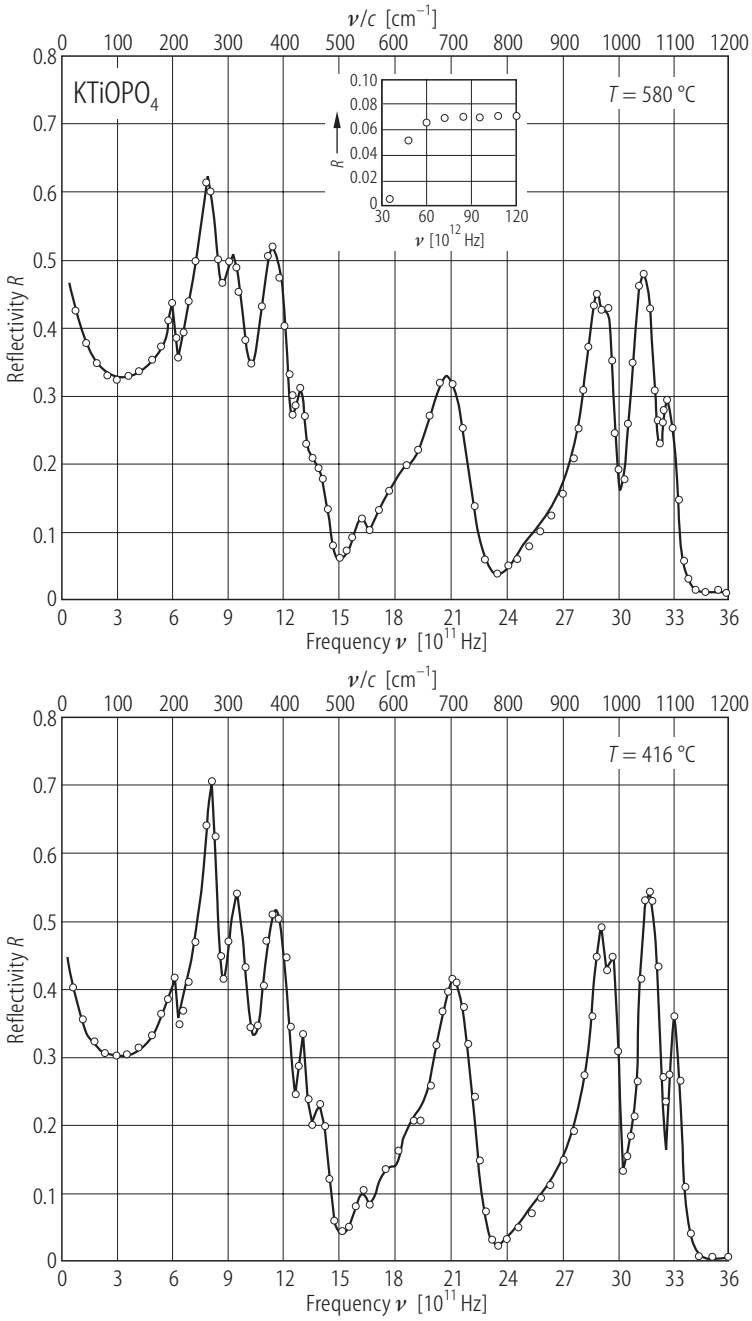

Fig. 35A-6-047. $KTiOPO_4$. R vs. ν [91Moh]. R: infrared reflectivity for A_1 symmetry species. Parameter: T. The lines show calculated results.

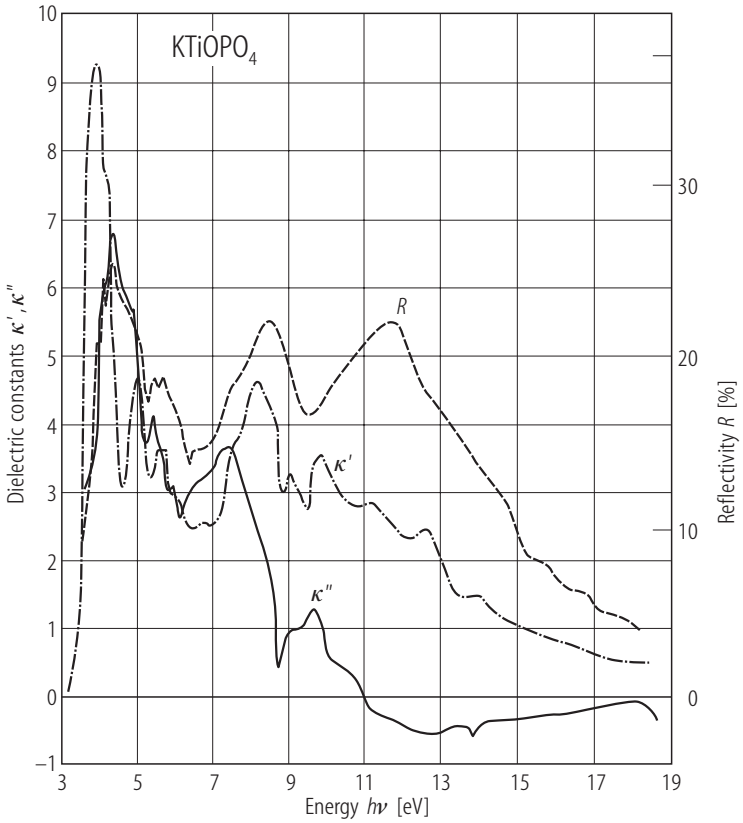

Fig. 35A-6-048. $KTiOPO_4$. R, κ', κ'' vs. $h\nu$ [91Dov]. R: reflectivity. $h\nu$: photon energy. $E \parallel z$.

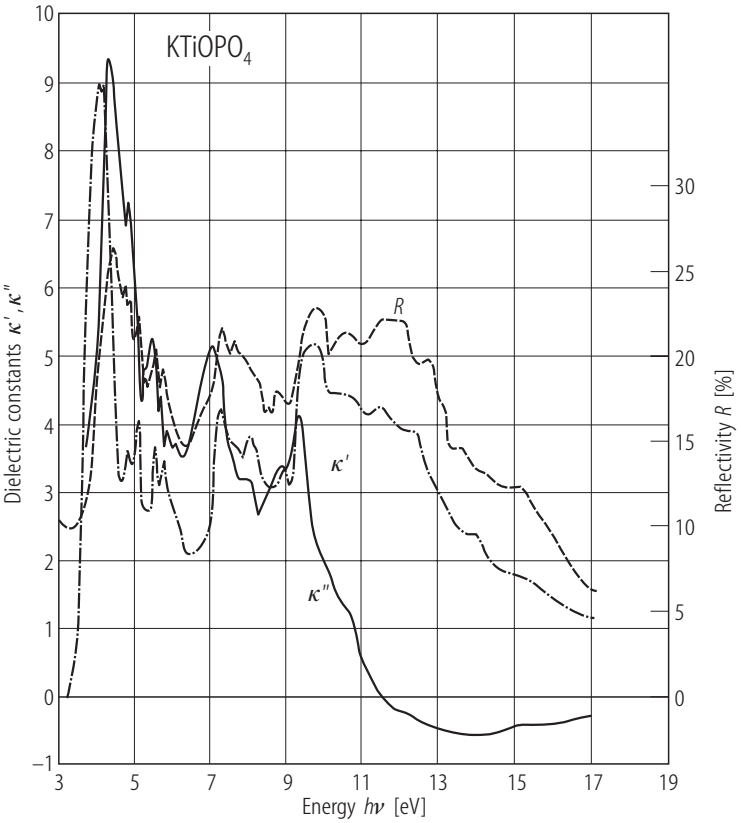

Fig. 35A-6-049. $KTiOPO_4$. R, κ', κ'' vs. $h\nu$ [91Dov]. R: reflectivity. $h\nu$: photon energy. $E \parallel x$.

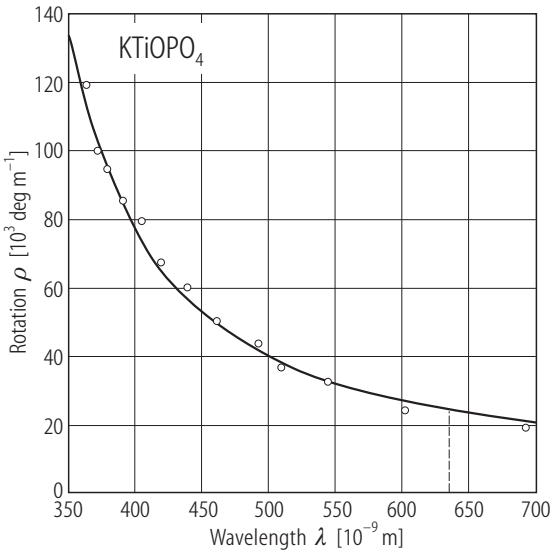

Fig. 35A-6-050. $KTiOPO_4$. ρ vs. λ [91Tho]. ρ: optical rotation.

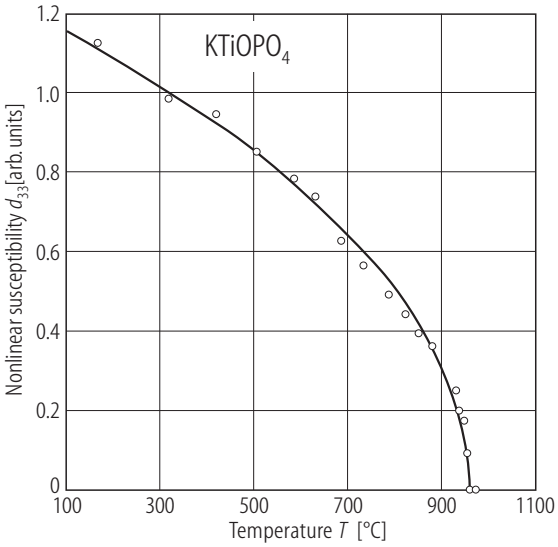

Fig. 35A-6-051. $KTiOPO_4$. d_{33} vs. T [92Chu]. $\lambda = 1.047$ µm. d_{33}: nonlinear susceptibility.

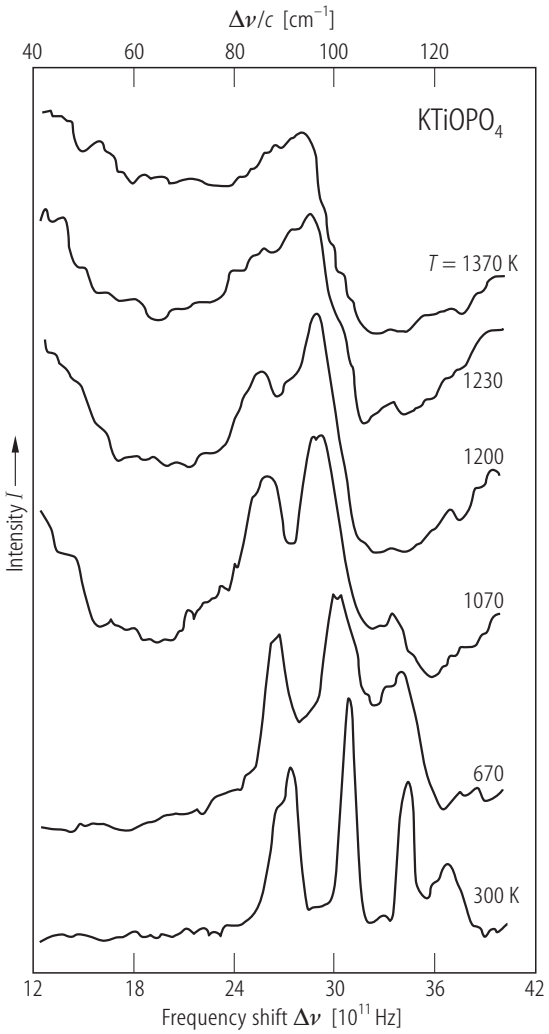

Fig. 35A-6-052. $KTiOPO_4$. I vs. $\Delta\nu$ [89Vor]. I: Raman scattering intensity. $\Delta\nu$: Raman shift. B_2(TO)-mode, $X(YZ)X$. Parameter: T.

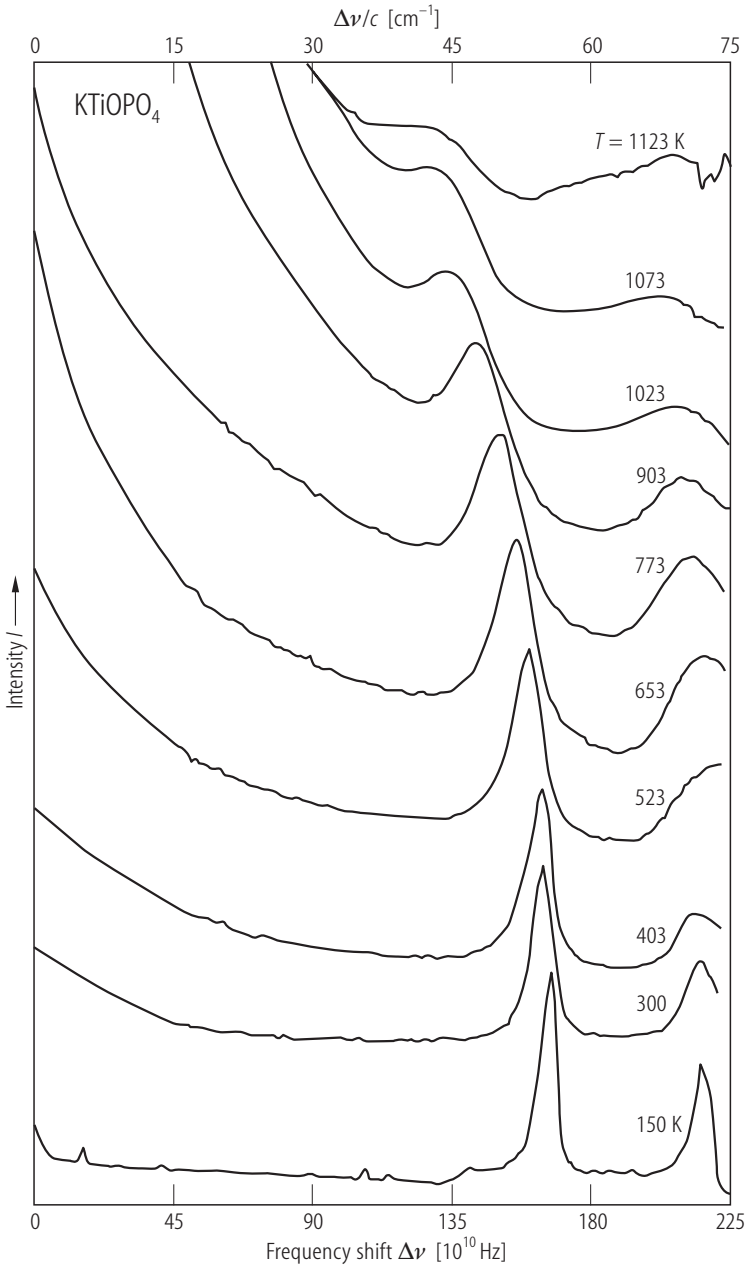

Fig. 35A-6-053. $KTiOPO_4$. I vs. $\Delta\nu$ [91Fur]. I: Raman scattering intensity. $\Delta\nu$: Raman shift. Geometry: $X(YX)Y$. Parameter: T.

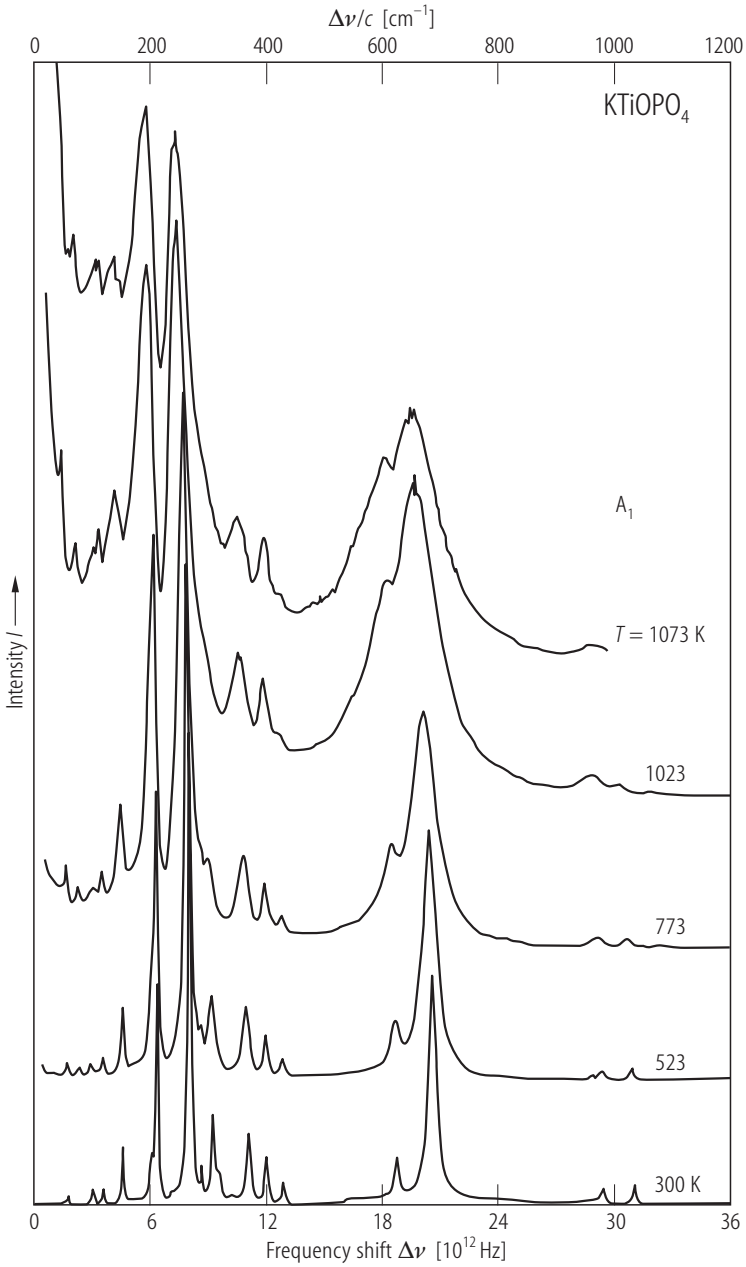

Fig. 35A-6-054. $KTiOPO_4$. I vs. $\Delta\nu$ [91Fur]. I: Raman scattering intensity. $\Delta\nu$: Raman shift. Geometry: $X(ZZ)Y$. Parameter: T.

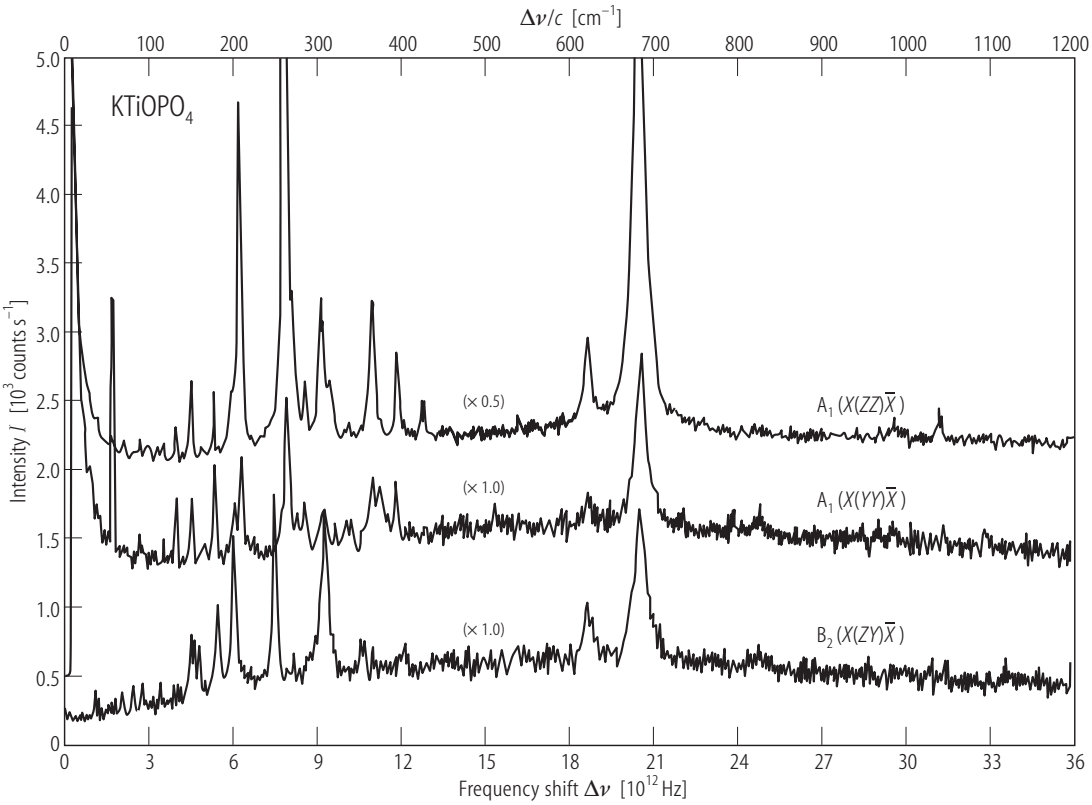

Fig. 35A-6-055. $KTiOPO_4$. I vs. $\Delta\nu$ [88Kug]. I: Raman scattering intensity. $\Delta\nu$: Raman shift. $T = 300$ K.

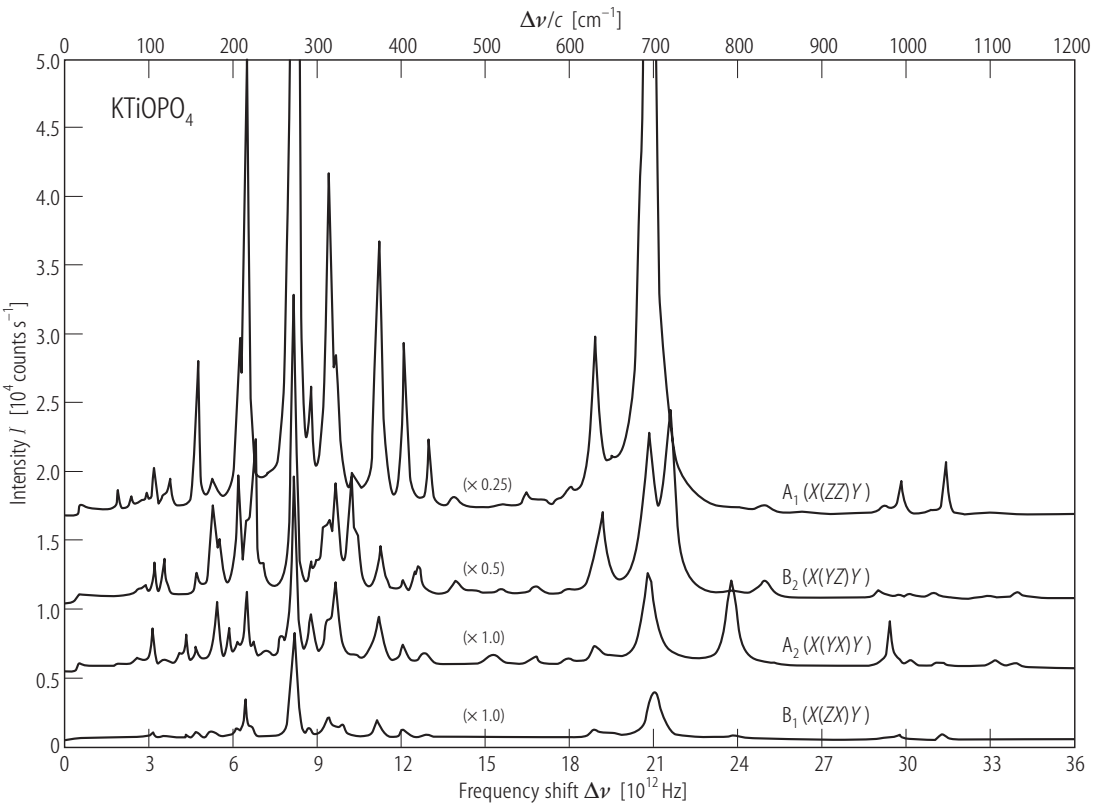

Fig. 35A-6-056. $KTiOPO_4$. I vs. $\Delta\nu$ [88Kug]. I: Raman scattering intensity. $\Delta\nu$: Raman shift. T = 300 K.

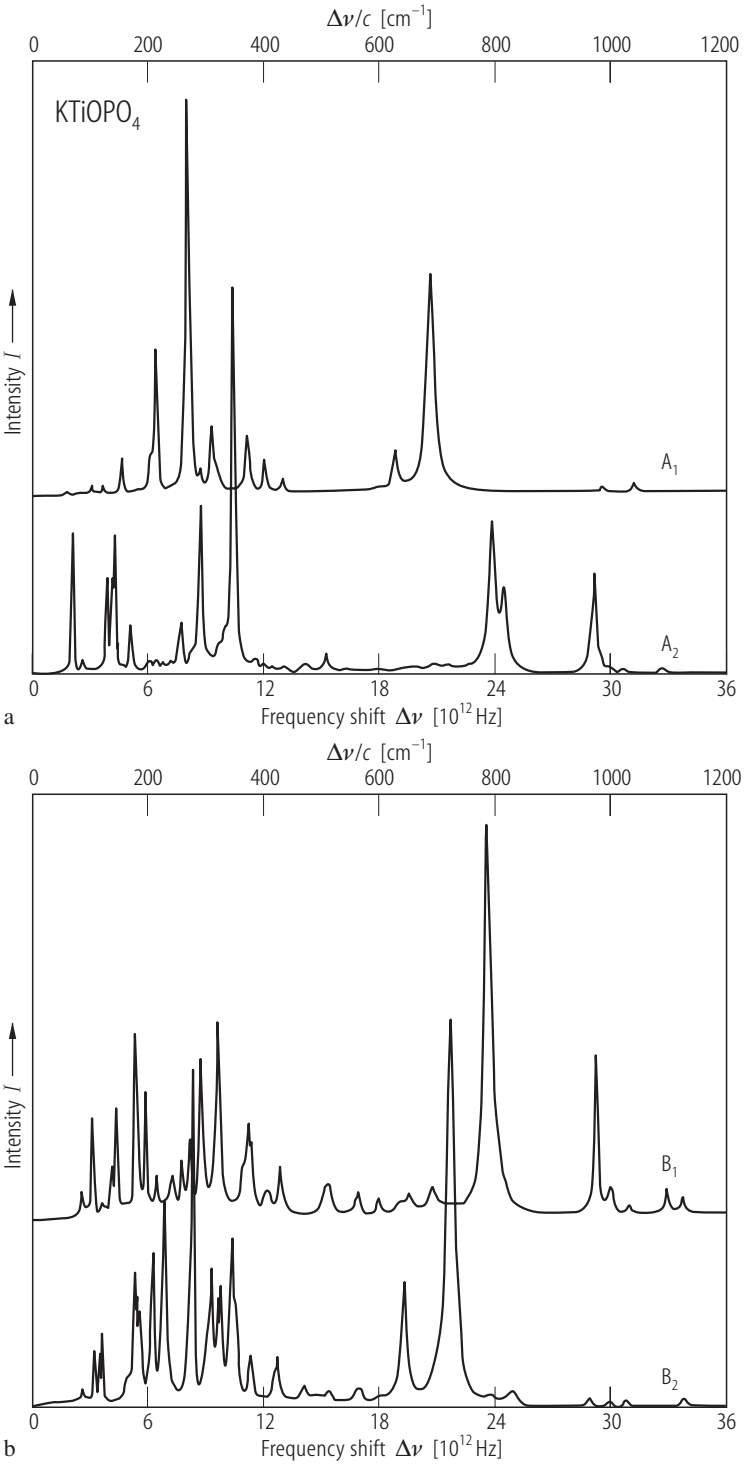

Fig. 35A-6-057. $KTiOPO_4$. I vs. $\Delta\nu$ [91Fur]. I: Raman scattering intensity. $\Delta\nu$: Raman shift. (**a**) A_1 mode: $X(ZZ)Y$, A_2 mode: $X(YX)Y$. (**b**) B_1 mode: $X(ZX)Y$, B_2 mode: $X(YZ)Y$.

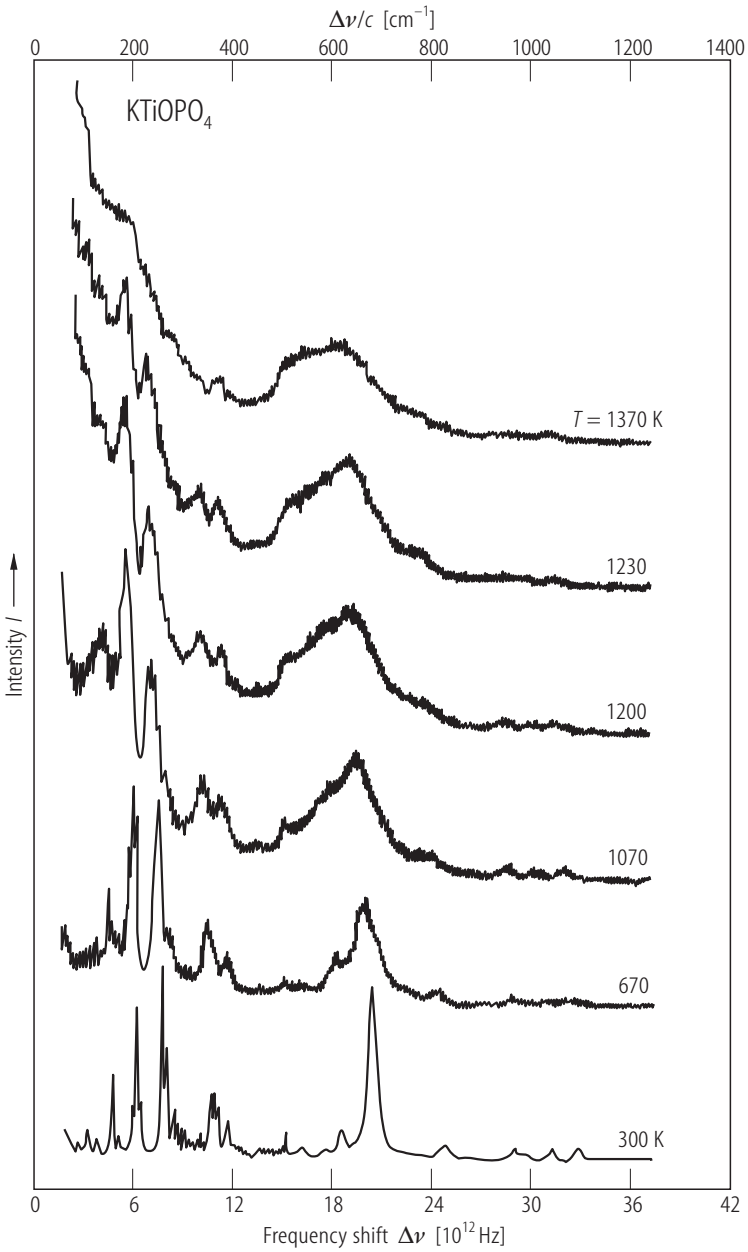

Fig. 35A-6-058. $KTiOPO_4$. I vs. $\Delta\nu$ [89Vor]. I: Raman intensity. $\Delta\nu$: Raman shift. A_1(TO)-mode, $X(YY)X$. Parameter: T.

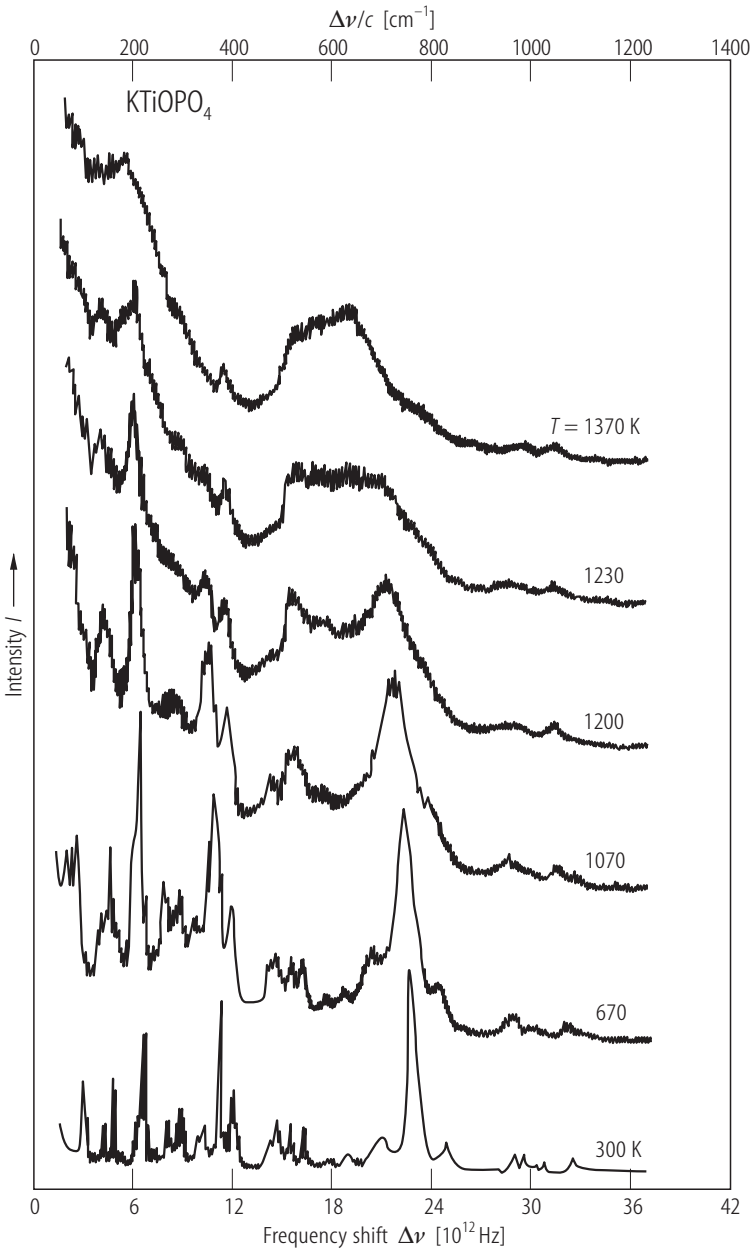

Fig. 35A-6-059. $KTiOPO_4$. I vs. $\Delta\nu$ [89Vor]. I: Raman intensity. $\Delta\nu$: Raman shift. A_1(LO)-mode, *Z(YY)Z*. Parameter: T.

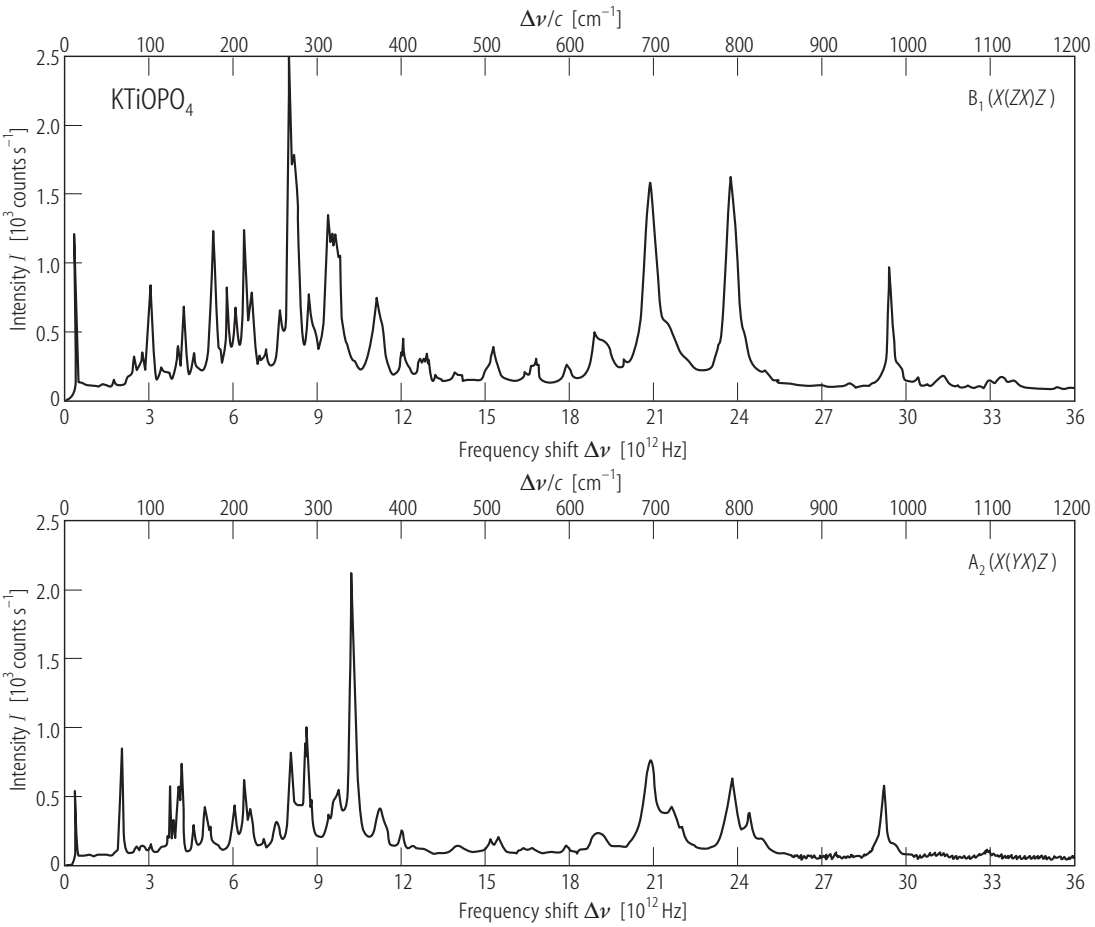

Fig. 35A-6-060. $KTiOPO_4$. I vs. $\Delta\nu$ [88Kug]. I: Raman intensity. $\Delta\nu$: Raman shift. T = 300 K.

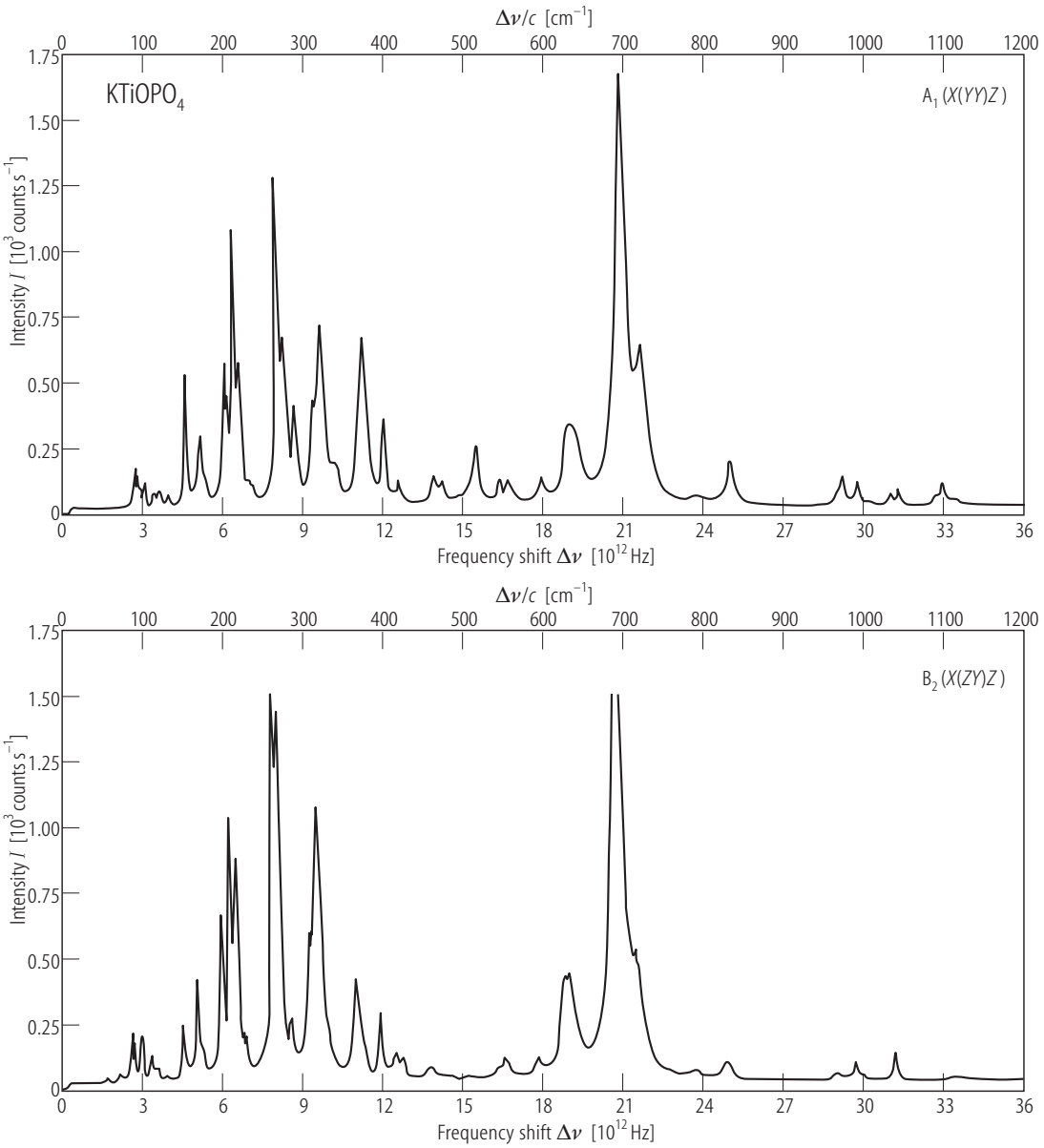

Fig. 35A-6-061. $KTiOPO_4$. I vs. $\Delta\nu$ [88Kug]. I: Raman intensity. $\Delta\nu$: Raman shift. $T = 300$ K.

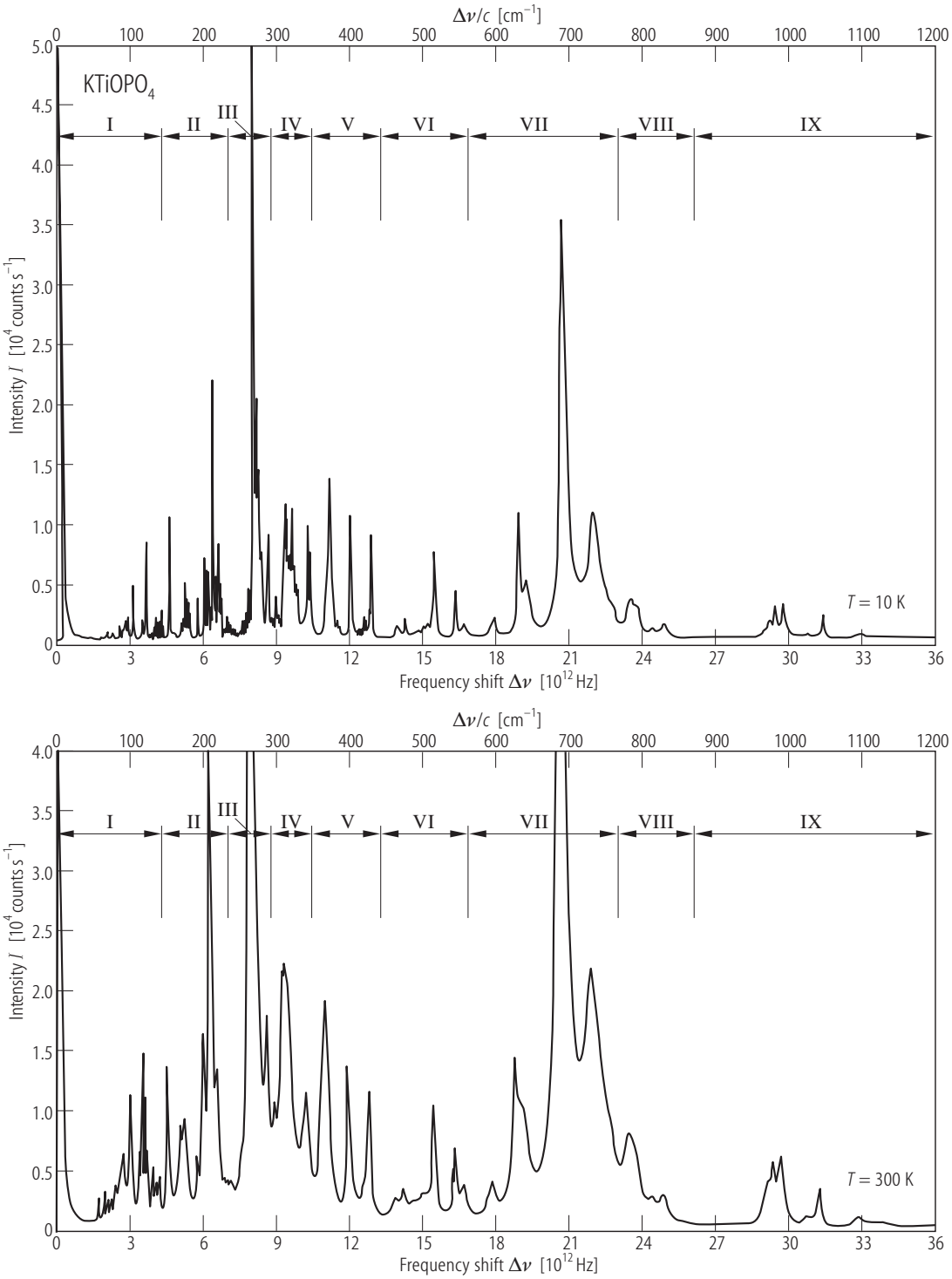

Fig. 35A-6-062. $KTiOPO_4$. I vs. $\Delta\nu$ [88Kug]. I: Raman intensity. $\Delta\nu$: Raman shift. Parameter: T. Scattering geometry: $X(ZX)Y$. The nine main frequency ranges (I–IX) are shown in Table 35A-6-020.

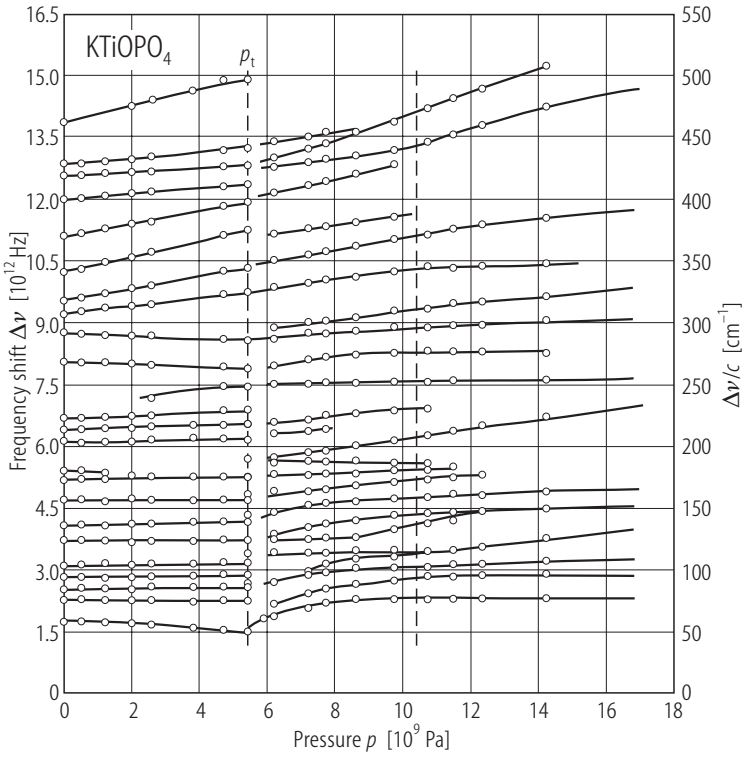

Fig. 35A-6-063. $KTiOPO_4$. $\Delta\nu$ vs. p [87Kou]. $\Delta\nu$: Raman shift. p_t: transition pressure.

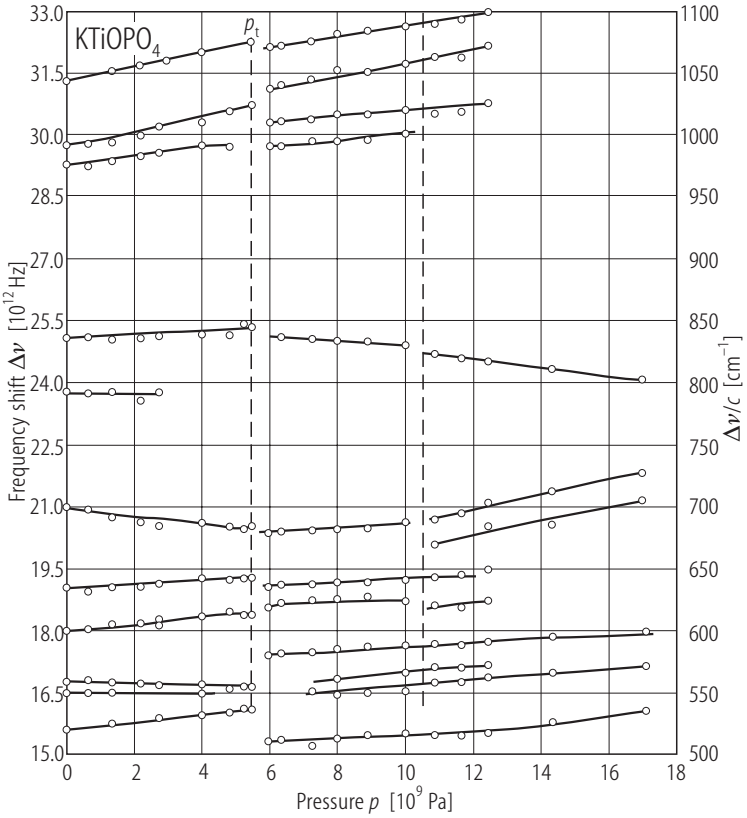

Fig. 35A-6-064. $KTiOPO_4$. $\Delta\nu$ vs. p [87Kou]. $\Delta\nu$: Raman shift. p_t: transition pressure.

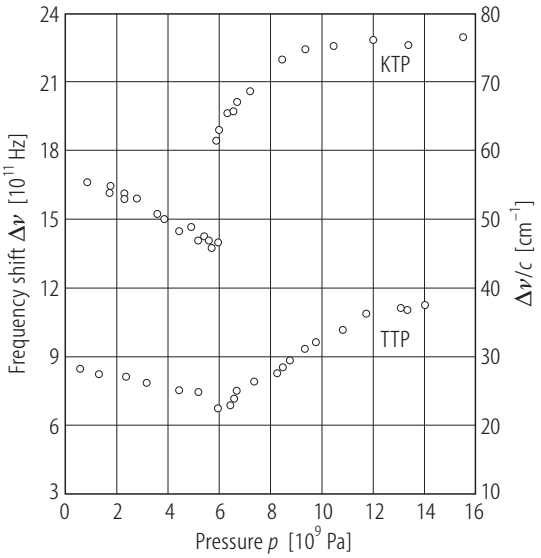

Fig. 35A-6-065. $KTiOPO_4$, $TlTiOPO_4$. $\Delta\nu$ vs. p [91Ser]. $\Delta\nu$: Raman shift. Scattering geometry: $X(ZZ)\overline{X}$.

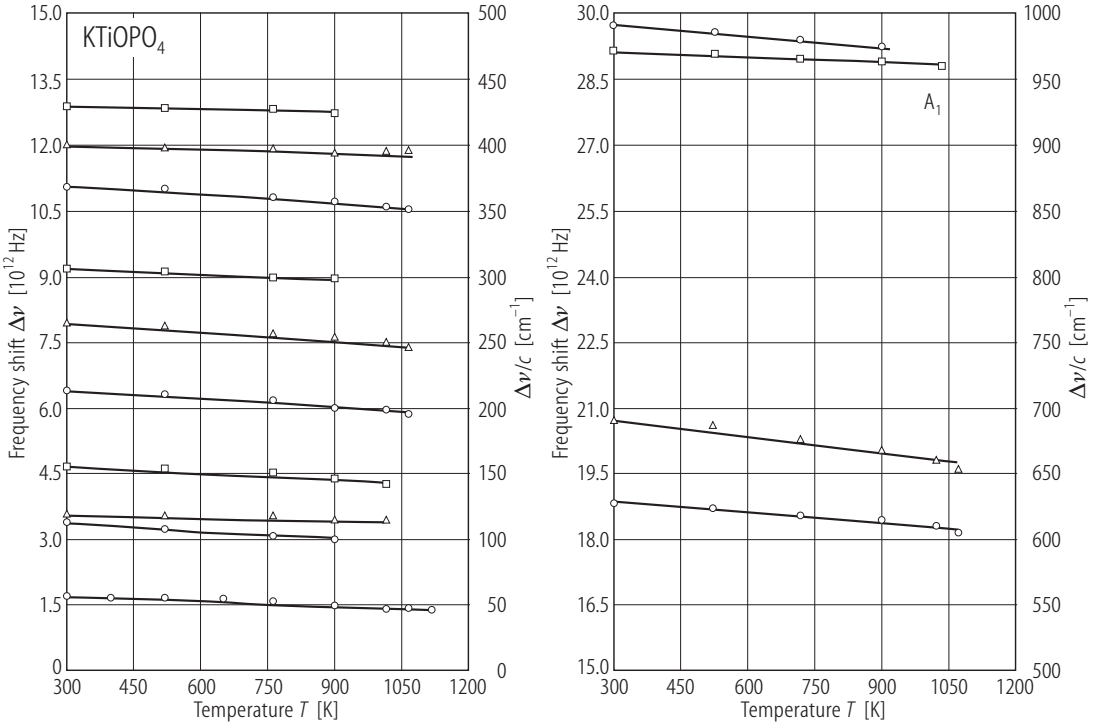

Fig. 35A-6-066. $KTiOPO_4$. $\Delta\nu$ vs. T [91Fur]. $\Delta\nu$: Raman shift. Geometry: $X(ZZ)Y$.

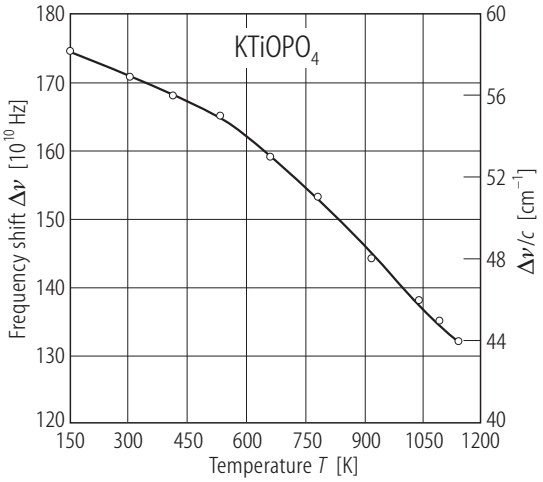

Fig. 35A-6-067. $KTiOPO_4$. $\Delta\nu$ vs. T [91Fur]. $\Delta\nu$: Raman shift. Geometry: $X(ZZ)Y$.

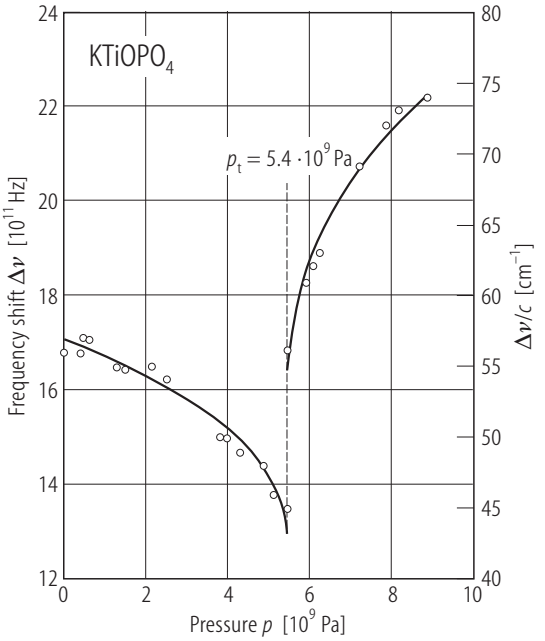

Fig. 35A-6-068. $KTiOPO_4$. $\Delta\nu$ vs. p [87Kou]. $\Delta\nu$: Raman shift. p_t: transition pressure.

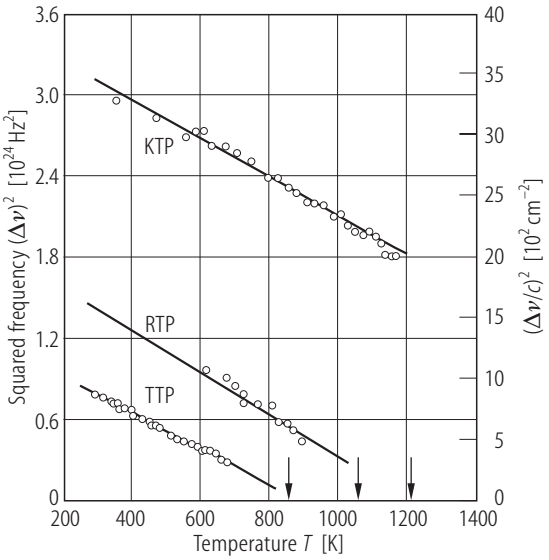

Fig. 35A-6-069. $KTiOPO_4$, $RbTiOPO_4$, $TlTiOPO_4$. $(\Delta\nu)^2$ vs. T [91Ser]. $\Delta\nu$: frequency of the soft Raman mode. Arrows indicate ferroelectric transition temperatures.

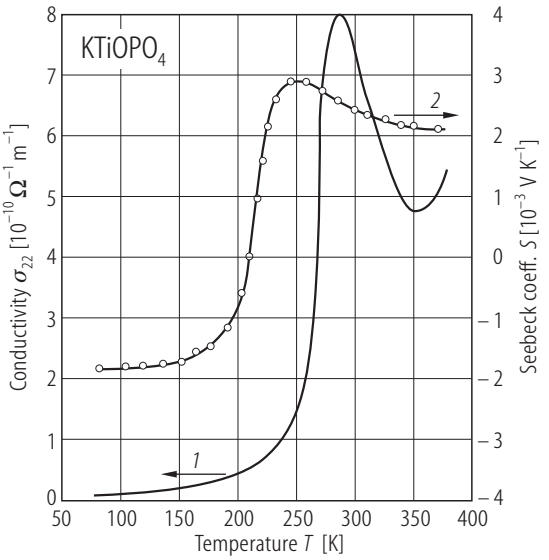

Fig. 35A-6-070. $KTiOPO_4$. σ_{22}, S vs. T [91Ant]. σ_{22}: conductivity along the y axis. S: Seebeck coefficient. f = 1 MHz.

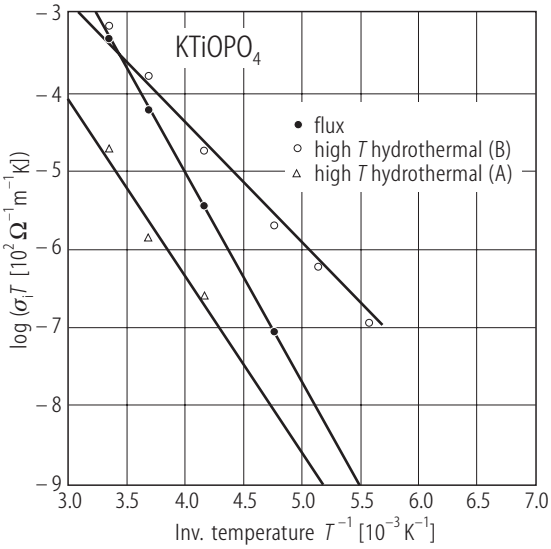

Fig. 35A-6-071. $KTiOPO_4$. $\log(\sigma_i T)$ vs. T^{-1} [90Mor]. σ_i: bulk ionic conductivity [$\cdot 10^2\ \Omega^{-1}\ m^{-1}$]. Growth techniques are indicated. A and B distinguish different origins.

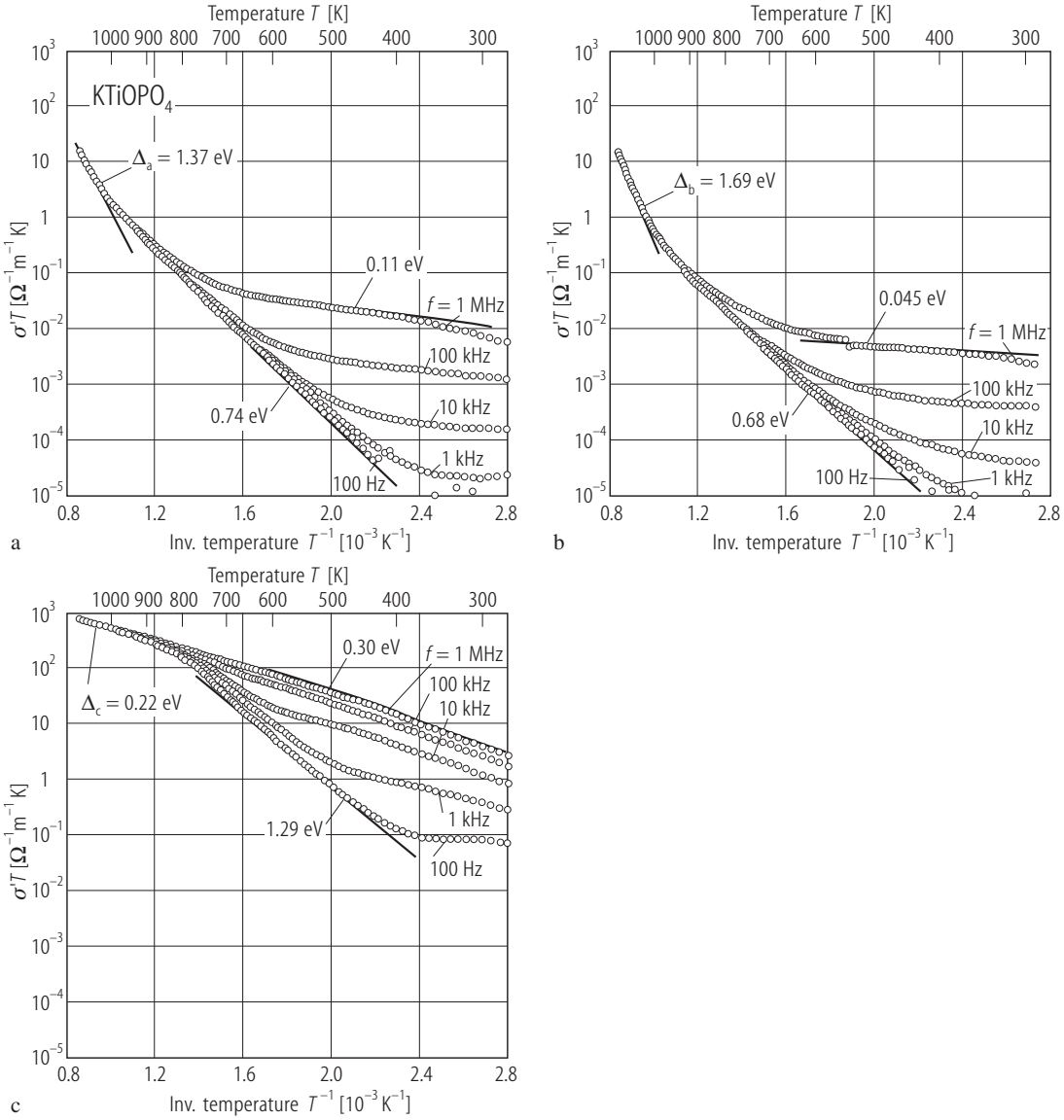

Fig. 35A-6-072. $KTiOPO_4$. $\sigma'T$ vs. T^{-1} [93Fur]. σ': real part of the complex conductivity. The slopes of the straight lines correspond to the average activation energies. (**a**) along [100] direction, (**b**) along [010] direction, (**c**) along [001] direction. Parameter: *f*.

Fig. 35A-6-073 *was misarranged. Therefore, it has been moved to No. 35A-11 as Fig. 35A-11-005.*

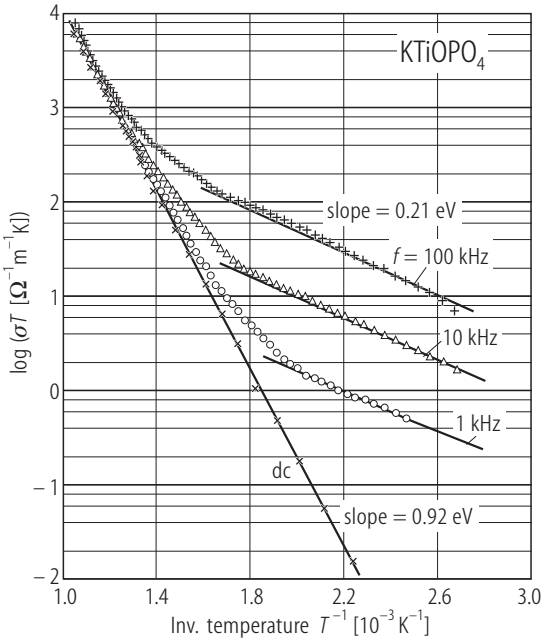

Fig. 35A-6-074. $KTiOPO_4$. $\log \sigma T$ vs. T^{-1} [92Cho]. Parameter: f. σ: electrical conductivity.

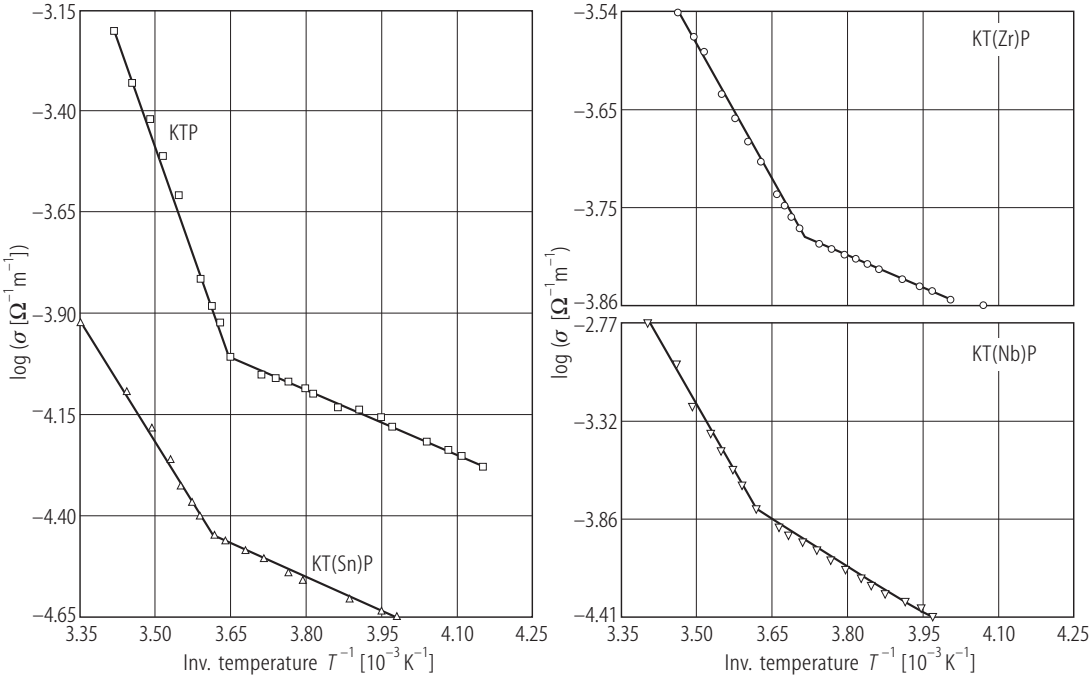

Fig. 35A-6-075. $KTiOPO_4$, $KTiOPO_4$:Nb (15 mol%), $KTiOPO_4$:Zr (15 mol%), $KTiOPO_4$:Sn (15 mol%). $\log \sigma$ vs. T^{-1} [92Sas]. σ: conductivity along the c axis at 1 kHz.

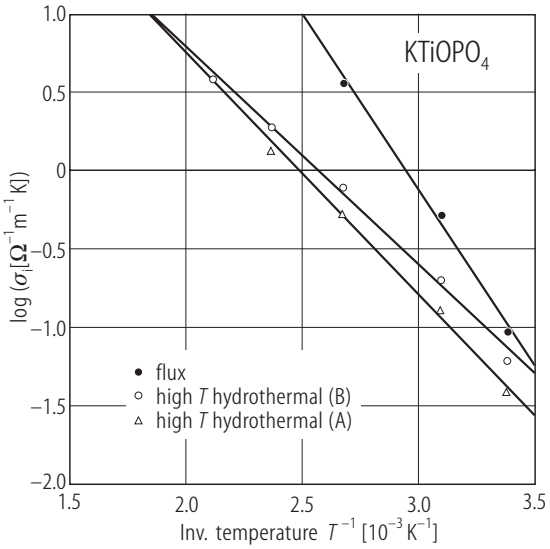

Fig. 35A-6-076. $KTiOPO_4$. $\log \sigma_i$ vs. T^{-1} [90Mor]. σ_i: bulk ionic conductivity. Growth techniques are indicated. A and B distinguish different origins.

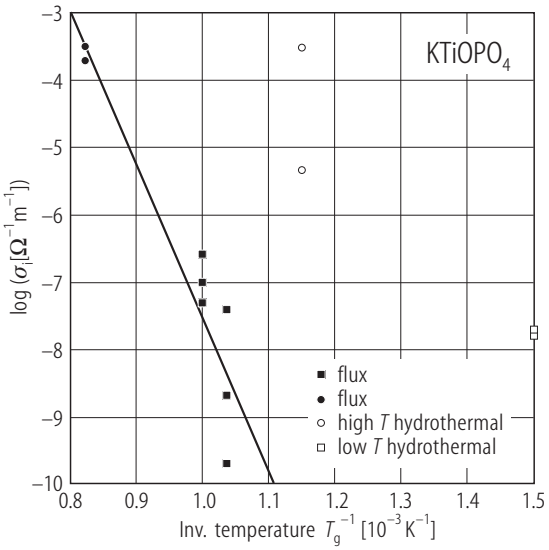

Fig. 35A-6-077. $KTiOPO_4$. $\log \sigma_i$ vs. T_g^{-1} [90Mor]. σ_i: bulk ionic conductivity at RT. T_g: growing temperature [K]. Techniques are indicated.

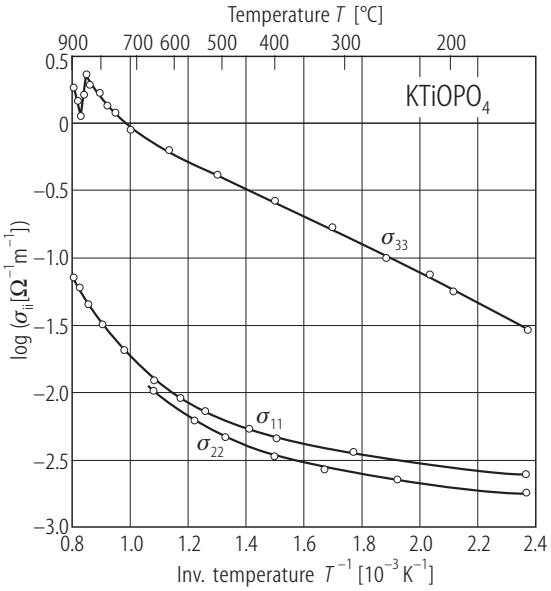

Fig. 35A-6-078. $KTiOPO_4$. $\log \sigma_{ii}$ vs. T^{-1} [88Vor]. σ_{ii}: electrical conductivity along the i th axis.

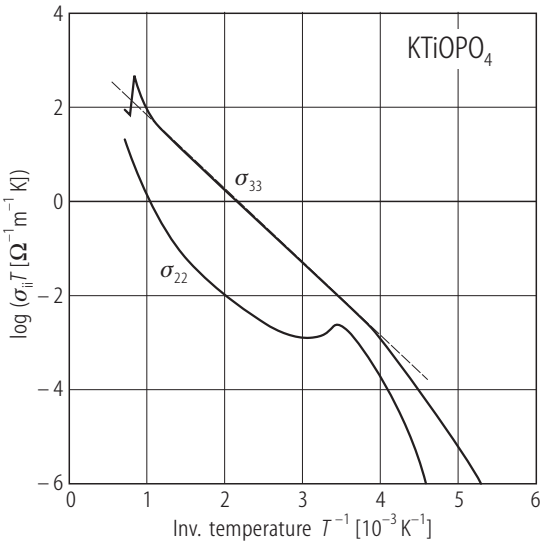

Fig. 35A-6-079. $KTiOPO_4$. $\log(\sigma_{22}T)$, $\log(\sigma_{33}T)$ vs. T^{-1} [91Ant]. f = 1 MHz. σ_{22}, σ_{33}: conductivity along the y- and z-axes, respectively.

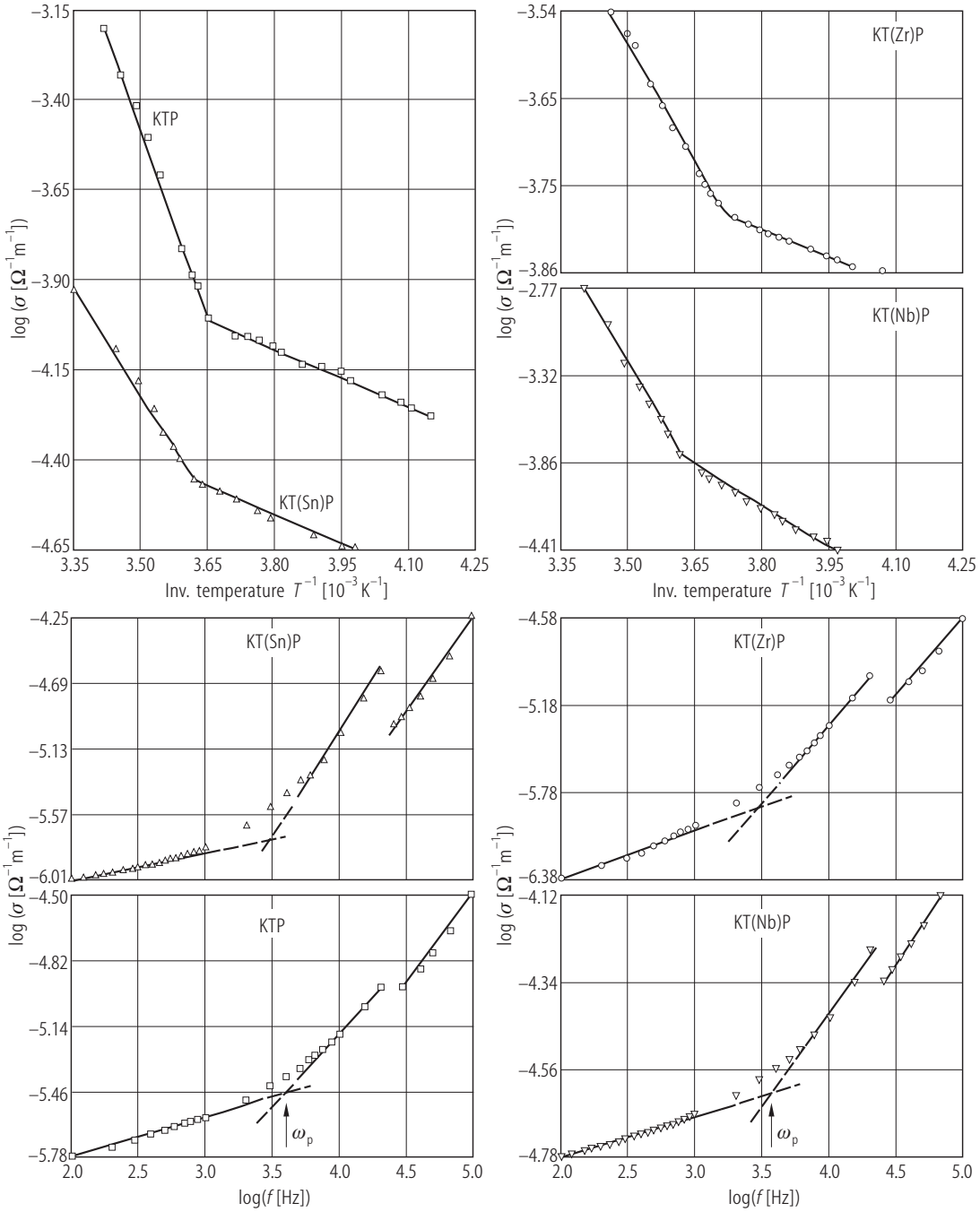

Fig. 35A-6-080. $KTiOPO_4$, $KTiOPO_4$:Nb (15 mol%), $KTiOPO_4$:Zr (15 mol%), $KTiOPO_4$:Sn (15 mol%). log σ vs. log f and T^{-1}, respectively [92Sas]. σ: conductivity along the c axis.

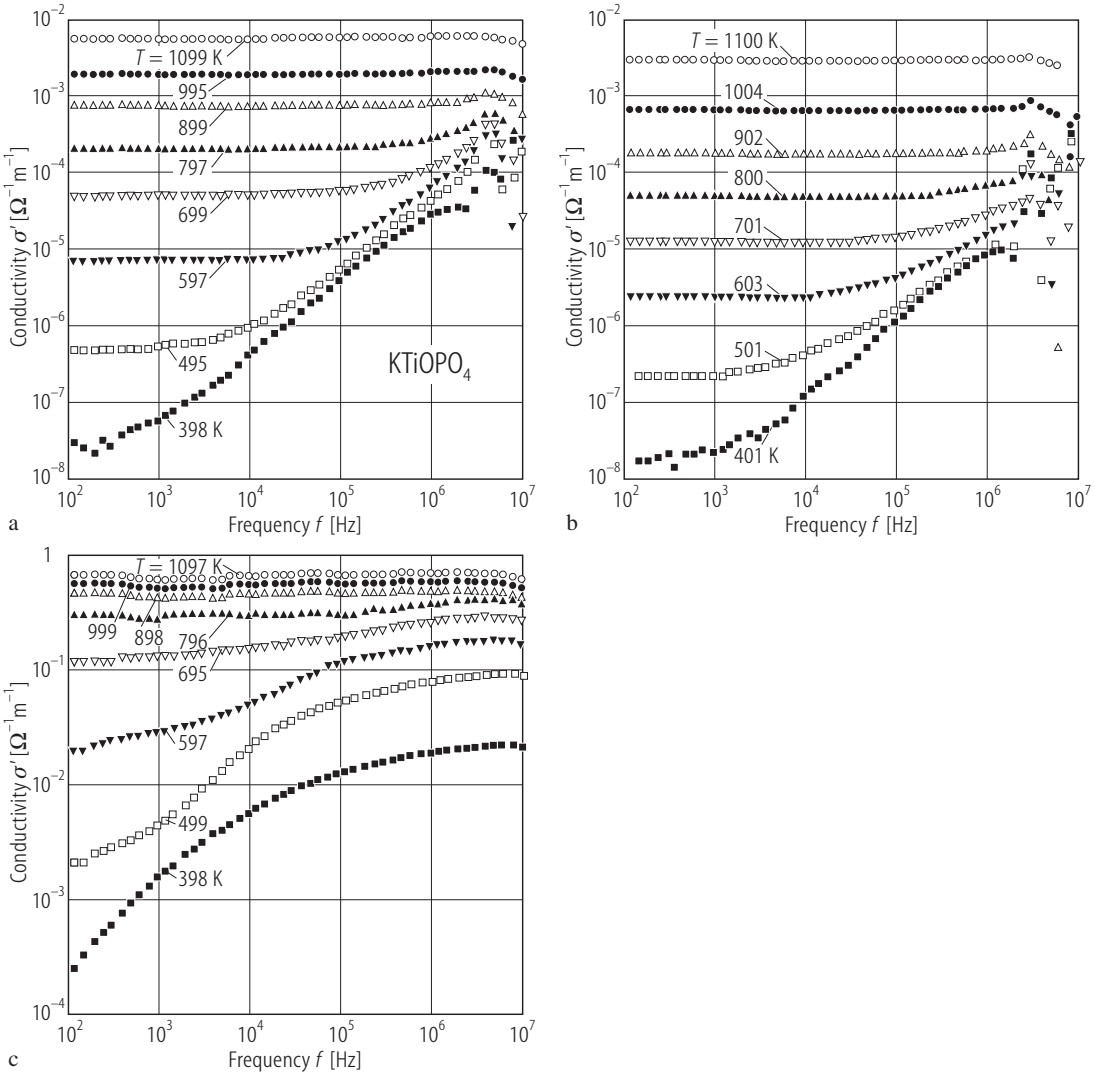

Fig. 35A-6-081. $KTiOPO_4$. σ' vs. f [93Fur]. σ': real part of the complex conductivity. (**a**) along [100] direction, (**b**) along [010] direction, (**c**) along [001] direction. Parameter: T.

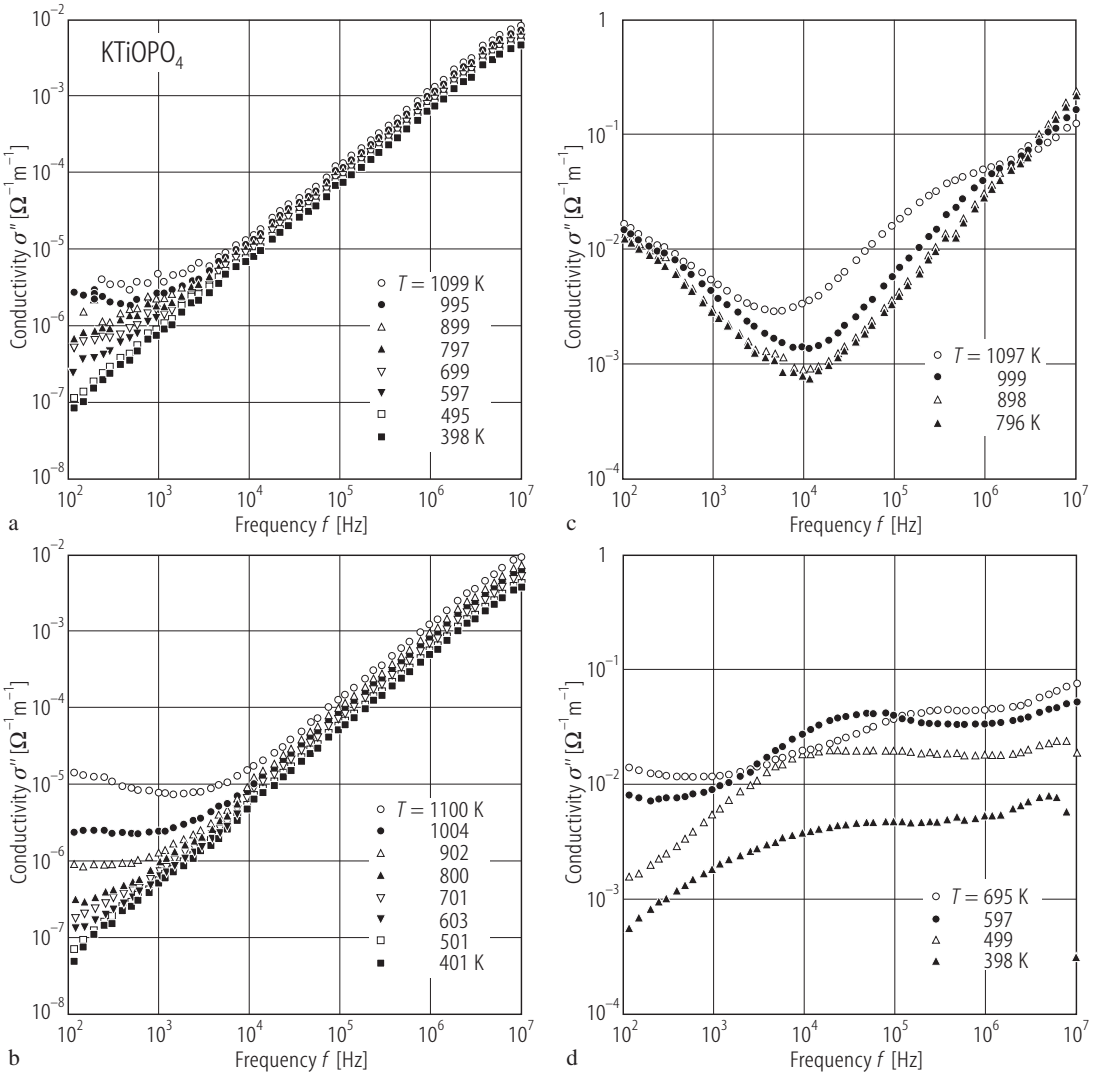

Fig. 35A-6-082. $KTiOPO_4$. σ'' vs. f [93Fur]. σ'': imaginary part of the complex conductivity. (**a**) along [100] direction (400...1100 K), (**b**) along [010] direction (400...1100 K), (**c**) along [001] direction (800...1100 K), (**d**) along [001] direction (400...700 K). Parameter: T.

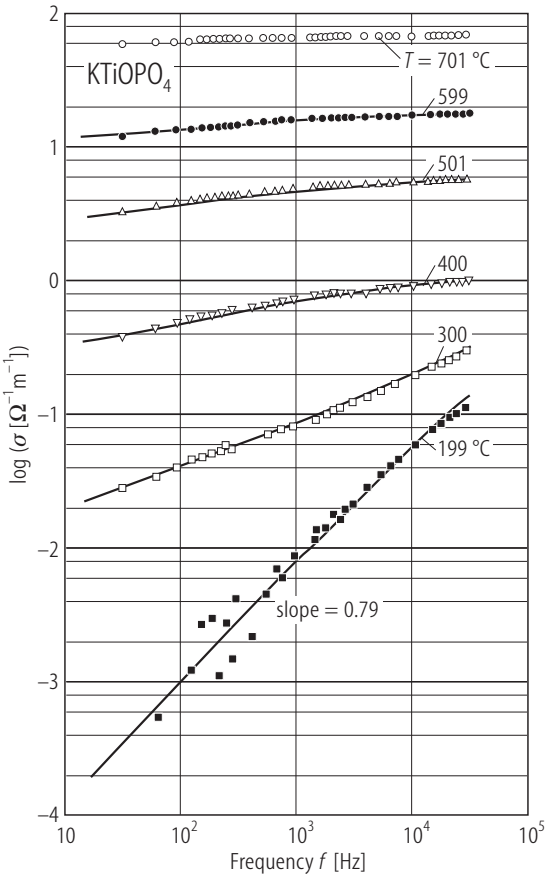

Fig. 35A-6-083. $KTiOPO_4$. log σ vs. f [92Cho]. Parameter: T. σ: electrical conductivity.

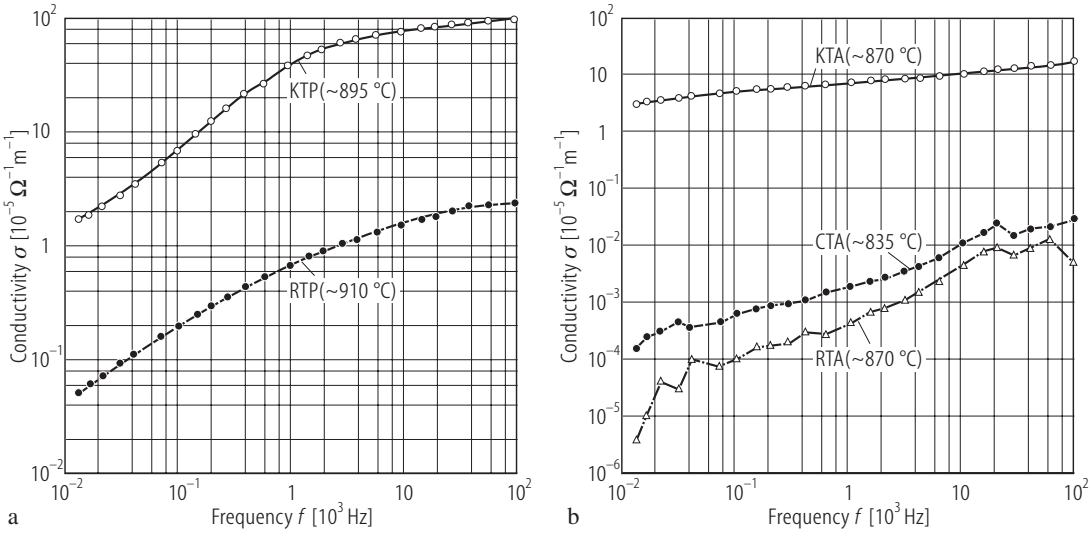

Fig. 35A-6-084. $KTiOPO_4$, $RbTiOPO_4$, $KTiOAsO_4$, $RbTiOAsO_4$, $CsTiOAsO_4$. σ vs. f [94Che1]. (**a**) Phosphates; (**b**) arsenates. *c*-plates. Average crystal growth temperature is shown in parentheses.

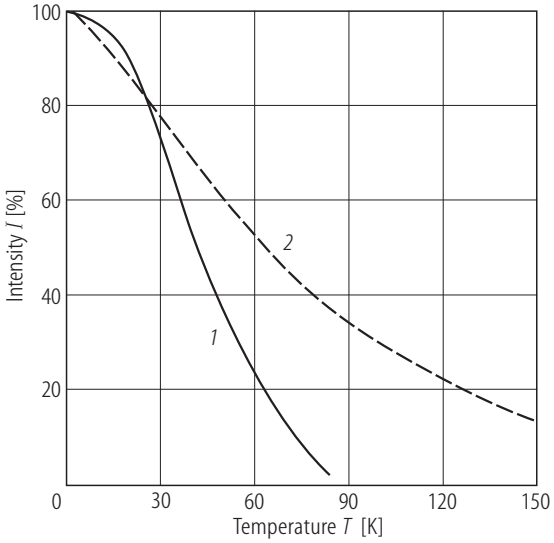

Fig. 35A-6-085. $KTiOPO_4$, $KTi_{0.98}Nb_{0.01}Ga_{0.01}OPO_4$. I vs. T [89Bla]. I: luminescence intensity with excitation light of $\lambda = 341$ nm. (*1*) $KTiOPO_4$; (*2*) $KTi_{0.98}Nb_{0.01}Ga_{0.01}OPO_4$.

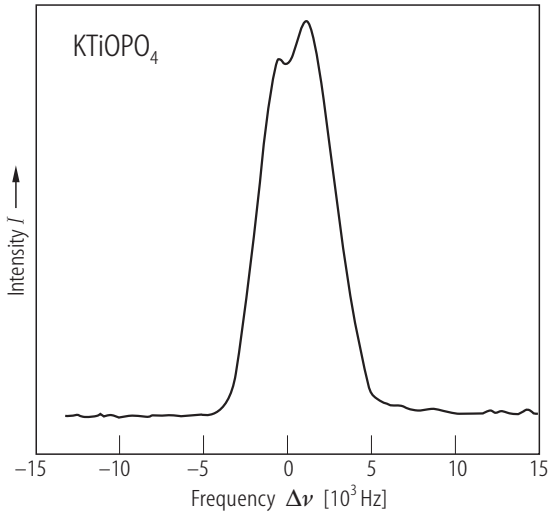

Fig. 35A-6-086. $KTiOPO_4$. I vs. $\Delta\nu$ [96Han]. I: ^{31}P NMR intensity. $\Delta\nu$: frequency relative to $\nu_L = 81$ MHz.

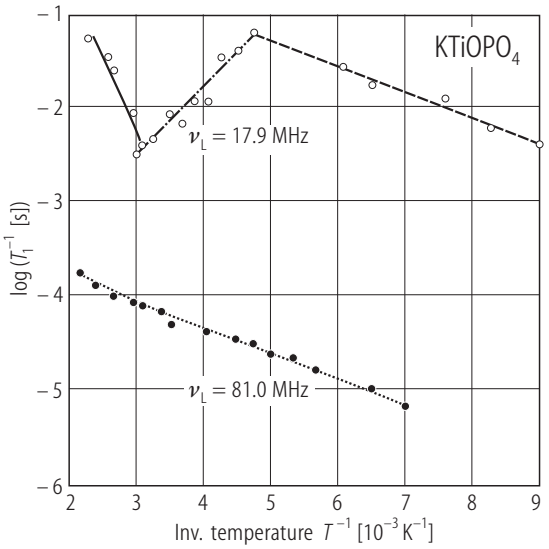

Fig. 35A-6-087. $KTiOPO_4$. $\log(T_1^{-1})$ vs. T^{-1} [96Han]. T_1: spin-lattice relaxation time [s] of ^{31}P nuclei. Parameter: ν_L.

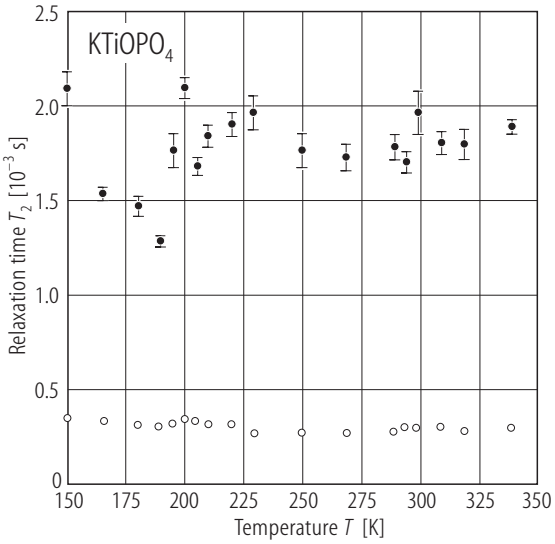

Fig. 35A-6-088. $KTiOPO_4$. T_2 vs. T [96Han]. T_2: spin-spin relaxation time of ^{31}P nuclei at ν_L = 81 MHz.

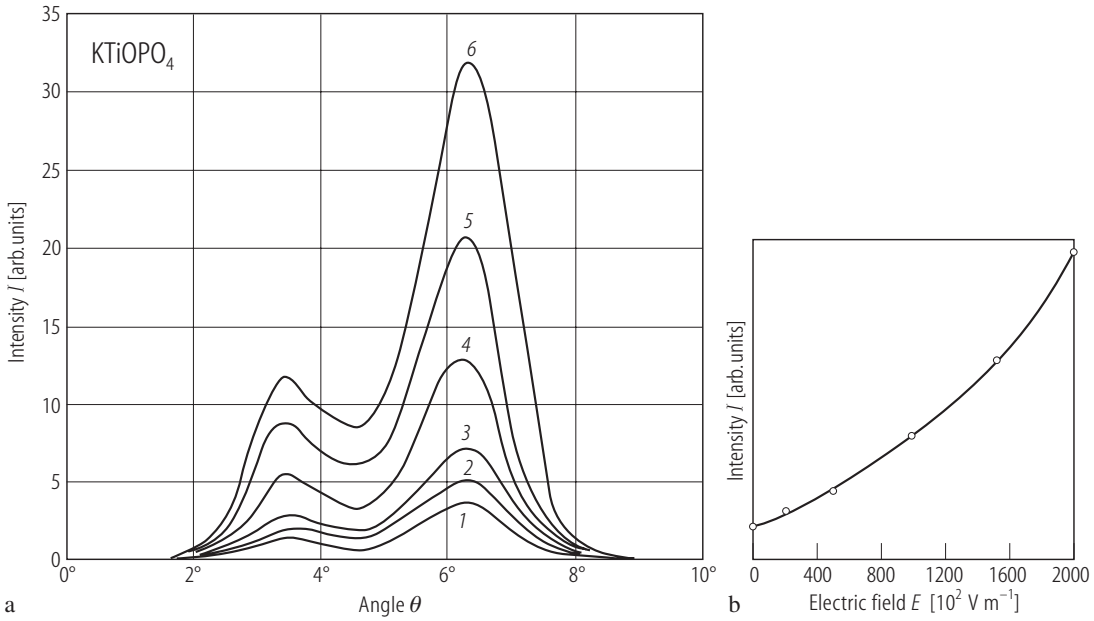

Fig. 35A-6-089. $KTiOPO_4$. (**a**) I vs. θ ((004) rocking curve recorded with and without in situ electric field along the [001] direction), (**b**) Peak intensity vs. E [92Seb]. (*1*) E = 0 kV m^{-1}, (*2*) 20 kV m^{-1}, (*3*) 50 kV m^{-1}, (*4*) 100 kV m^{-1}, (*5*) 150 kV m^{-1}, (*6*) 200 kV m^{-1}. The duration of the experiment was about 30 min. After switching off the field, the intensity approximately returned to curve (*1*). θ: increment of the diffraction angle.